The NMR Chemical Shift: Insight into Structure and Environment

ANGEL C. de DIOS

Department of Chemistry, University of Illinois at Urbana-Champaign, 505 South Mathews Avenue, Urbana, Illinois 61801, USA

CYNTHIA J. JAMESON

Department of Chemistry M/C 111, University of Illinois at Chicago, 845 W. Taylor, Chicago, Illinois 60607, USA

ANNUAL REPORTS ON NMR SPECTROSCOPY
VOLUME 29 ISBN 0-12-505329-0

1. INTRODUCTION

The NMR chemical shift is well known to be extremely sensitive to the environment of the nucleus. The chemical shift of a methyl proton is in a region of the proton shift that is well separated from the chemical shift of a proton in a CH_2 group, for example. Furthermore, the two protons in a CH_2 group could have distinct chemical shifts depending on the immediate neighbouring atoms of each proton. The ease of discrimination between *cis* and *trans*, *syn* and *anti* even under the lower resolution of the early spectrometers, was well known. With present-day instrumentation even subtle differences are easily observed. The NMR chemical shift discriminates between S and R enantiomers in a chiral solvent and between the various alanine residues in the same protein molecule, for example. There is no other property that has this degree of sensitivity to the electronic environment. In condensed phases there are gas-to-liquid shifts or solvent shifts, matrix-induced chemical shifts, site-dependent shielding tensors in crystalline solids, and adsorption shifts for molecules on surfaces. The Xe chemical shift of xenon gas trapped in the channels and cages of zeolites exhibits large changes with type of zeolite, and for the same zeolite it is found to be extremely dependent on the amount of adsorbed xenon, changing with loading in a way that is unique for each zeolite type so that such behaviour serves as a fingerprint of zeolites. There are no changes in molecular geometry or bonding involved here, merely the effects of neighbouring atoms on the Xe chemical shift, that is, the oxygen atoms of the framework, the counter-ions, and the other Xe atoms that it encounters in the intrazeolitic pores. Even where the average distance between neighbouring atoms is extremely large, as in the dilute gas phase, the NMR chemical shift is found to change with this average distance, exhibiting a dependence on the density and the temperature. This second virial coefficient of shielding can be measured more accurately than the second virial coefficient of any other molecular electronic property. When the chemical shift in a molecule in the gas phase is extrapolated to zero density, one would expect to obtain the chemical shift of an effectively isolated molecule, with no neighbour effects. This too is found to be changing with temperature. Furthermore, when a molecule is observed in the same solution with its deuterated counterpart, a nucleus in the heavier isotopomer is usually more shielded than the same nucleus in the lighter isotopomer. This isotope shift is sometimes observed even when the NMR nucleus and the site of isotopic substitution are separated by several bonds, as many as nine or more bonds, the signs and magnitudes of the isotope shifts changing across the periodic table.

How do we explain these observations? We shall see that these phenomena are due to the dependence of the nuclear shielding on the configuration of the nuclei, the distances between them, the bond angles and torsion angles between them; in other words, we shall consider the multidimensional shielding surface which describes the variation of the shielding with nuclear positions, analogous to the potential energy multidimensional surface. Not only is the value on this shielding surface at the minimum energy (equilibrium) geometry closely associated with the value that is observed, but the averaging over this surface during the rotation, vibration, and translational motions of the nuclei determines the shielding value that is observed. The observed chemical shift is averaged not only over all the populated rovibrational states, torsions and librations, but also over all the ensembles of the molecule with its neighbours in the gas or solution or adsorbed fluid on a heterogeneous surface. No other molecular electronic property has been characterized so well in terms of the virial coefficients, the mass dependence, and the temperature dependence. The ultra-high resolution afforded by the NMR measurement combined with the exquisite sensitivity of the shielding together make it possible to characterize this molecular property in detail experimentally. The change of the electric dipole polarizability with internuclear separation in a rare gas pair, for example, is one of the "pair interaction properties" that serve very well as tests of theories and physical models but are very difficult to measure. Contrast this with the ^{129}Xe shielding as a function of density and temperature in the dilute gas. Few property surfaces have been explored in their dependence on intramolecular nuclear coordinates. The only electronic property that has a well-known dependence on bond length is the dipole moment, and then only for a diatomic molecule. The experimental observations of the temperature dependence in the rotating–vibrating isolated molecule and the changes upon substitution of a remote atom by a heavier isotope are well characterized in the chemical shift, unlike any other molecular electronic property. The theories associated with the rovibrational averaging of any electronic property can be tested for this property, where both experiments and theoretical calculations are feasible. In other words, the NMR shielding serves as a paradigm for the exploration of the dependence of a molecular electronic property on intramolecular coordinates and masses, as well as intermolecular separations, dependence on the temperature, electric fields and field gradients, and grand ensemble configurations.

In this review we will consider nuclear shielding surfaces in simple systems: diatomic molecules to focus on the variation with bond length, H_2O, NH_3, PH_3 and CH_4 to consider bond angles and bond lengths, CH_3CH_3 through isobutane to see the dihedral angle dependence and bond angle effects. The variations with ϕ, ψ and χ angles are explored in various model peptides, and finally the remote bond stretches. Following the intramolecular shielding surfaces we move on to intermolecular shielding in atom–atom pairs, atom–ion, and atom–molecule pairs, and clusters of three or more, including up to five or 16 polar solvent molecules. The effects of

electric fields and electric field gradients on shielding are considered separately. Finally we tie these all together in an examination of possible global shapes of the traces on shielding surfaces. Dynamic averages over these surfaces are necessary for comparisons with experiment. Here we show the origin of the temperature dependence, the isotope shifts, the shifts with density and solvent, and hydrogen-bonding shifts. Ensemble averages are sometimes necessary to account properly for the observed cluster shifts and the average chemical shifts under fast exchange in porous media. Finally, we consider the prognosis for more complex systems. What can we say, in general, from the studies on these systems that may shed some light on shielding in more complex systems? How may the methods applicable to small systems be brought to bear on the prediction of chemical shifts in complex materials such as proteins where some electrostatics, some hydrogen bonding, some local bond angle and torsional constraints, and some long-range contributions apply?

2. SHIELDING SURFACES

A shielding surface is a mathematical surface providing the nuclear shielding value (usually the isotropic average over all magnetic field directions, but may also be an individual tensor component) as a function of the nuclear coordinates of the system. In the case of an isolated molecule, the intramolecular shielding surface is usually expressed in terms of nuclear displacement coordinates, such as curvilinear internal coordinates or the symmetry adapted linear combinations of these, the symmetry coordinates. In the case of intermolecular shielding surfaces, the internal coordinates of the supermolecule are used and the shielding is expressed relative to the completely separated interacting molecules including counterpoise corrections. The theoretical shielding surfaces that will be discussed in this review have been calculated using a variety of methods. The conventional Coupled Hartree Fock (CHF) method involves using a common gauge origin in the calculation and generally requires a larger set of basis functions to achieve the gauge independence. This method has been developed by Stevens, Pitzer and Lipscomb,[1] and by Lazzeretti and Zanasi.[2] At the next level the common origin method is employed in Second Order Polarization Propagation Approach (SOPPA) primarily by Oddershede and coworkers[3] and in Coupled MP2 by Bishop and Cybulski,[4] traditionally using large basis sets to achieve gauge independence. There are several distributed gauge origin approaches: the localized orbital local origin method (LORG) devised by Hansen and Bouman,[5] and its correlated level called SOLO (Second Order LORG),[6] the Individual Gauge for Localized Orbitals (IGLO) which has been developed by Schindler and Kutzelnigg,[7] and its correlated version MC-IGLO by van Wüllen and Kutzelnigg,[8] and a third method, Gauge-

including Atomic Orbitals (GIAO) originally introduced by Ditchfield,[9] used extensively by Chesnut, made more efficient by Wolinksi, Hinton and Pulay,[10] and rederived especially for correlated calculations by Gauss in MP2-GIAO.[11] The review by Chesnut in this volume[12] discusses the recent developments in these *ab initio* methods, and is not a subject of the present review. Our main concern is the resulting shielding surfaces, calculated by one of these methods at some appropriate basis set size. Theoretical calculations of nuclear shielding surfaces for small molecules have been reviewed recently.[13]

2.1. Intramolecular shielding surfaces

2.1.1. Dependence on bond length in diatomic molecules

The first complete shielding surface was calculated for the H_2^+ molecule by Hegstrom.[14] This surface showed the nuclear shielding for the separated atoms, all the way from 22 a.u. to the united atom, which in this case was an He^+ ion. From the large positive united atom value, the shielding is found to decrease until it reaches a minimum which occurs at an internuclear separation much longer than the equilibrium bond length and proceeds to the limiting value at infinite separation. Prior to this complete surface, however, the behaviour of the shielding in diatomic molecules in the immediate vicinity of the equilibrium geometry had already been discovered in the calculations by Stevens and coworkers for LiH,[15] HF,[16] CO,[17] and N_2.[18] The derivative of the shielding with bond distance was found to be negative in all cases except for the Li nucleus in LiH. Ditchfield's calculations of shieldings in the vicinity of the equilibrium bond length verified these results for LiH and for HF, and in addition provided similar results for the H_2 molecule.[19] Chesnut evaluated first derivatives of the shielding for the first- and second-row hydrides and found similar results for H_2, HF and HCl: NaH behaved similarly to LiH[20] and the second derivatives in HCl and HF,[21] as well as CO, N_2, CN^-, and F_2,[22] were also negative for all nuclei. That is, both nuclei in the diatomic molecule become deshielded as the bond lengthens, with the exception of the Li and the Na nuclei in LiH and NaH. The unusual behaviour of the alkali nuclei remained a puzzle until the complete shielding surface of the NaH molecule was calculated by Jameson and de Dios.[23] The complete surface for ^{23}Na in the NaH molecule looks very similar to the shielding surface for the H_2^+ molecule, as shown in Fig. 1. The equilibrium internuclear separation occurs at a bond length shorter than that separation at which the shielding is a minimum in H_2^+, as it does for the nuclei in diatomic molecules mentioned above and also for ClF.[23] On the other hand, the equilibrium internuclear separation occurs at a distance longer than that for the minimum in the shielding surface of the Na nucleus in the NaH molecule.

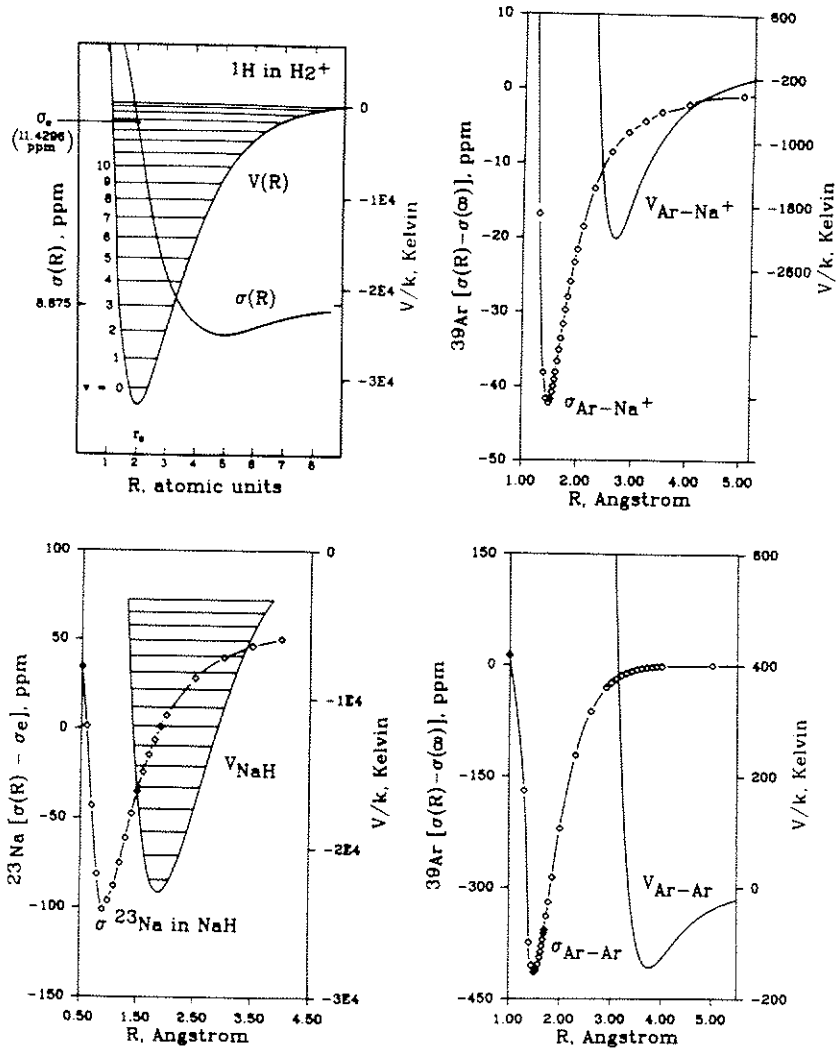

Fig. 1. Nuclear shielding surfaces from *ab initio* calculations. Reproduced from Ref. 23, with permission. The H_2^+ surface is from Hegstrom,[14] the ^{23}Na in NaH surface is from Ref. 23, and the ^{39}Ar in Ar–Na^+ and Ar–Ar intermolecular shielding surfaces are from Ref. 24. The last three were calculated using the LORG method.[25] The corresponding potential energy surfaces are from Wind,[26] Giroud and Nedelec,[27] Viehland,[28] and Aziz and Chen,[29] respectively.

2.1.2. Bond extension and angle deformation in small molecules

For triatomic and larger polyatomic molecules, the shielding surface is of higher dimension. The surface is best expressed in the nuclear displacement coordinates of the molecule, such as symmetry coordinates. Derivatives evaluated at the equilibrium geometry are, of course, easily converted from one set of coordinates to another. Examination of the details of the shielding surface is best carried out by displaying traces on the surface corresponding to keeping some of the coordinates constant. This was done for the first time by Raynes and coworkers for the nuclei in the H_2O molecule,[30] followed by the nuclei in the CH_4 molecule.[31] Jameson, de Dios and Jameson calculated the shielding surfaces for the N nucleus in NH_3[32] and P in PH_3.[33] In these calculations the inversion coordinates of both NH_3 and PH_3 were explored over a wide range of values.[32,33] When examined together (Fig. 2), these four surfaces have some features in common. The shielding of the non-H nuclei uniformly decreases with an increase in the symmetric stretch coordinate. The asymmetric stretch coordinates and the asymmetric angle deformation coordinates have zero first derivatives by symmetry, and therefore these traces are symmetric functions with respect to positive or negative displacements away from the equilibrium coordinates. They are concave in opposite directions. One (the asymmetric stretch) is concave downward (deshielding with increasing displacement from equilibrium), whereas the other (the asymmetric angle bend) is concave upward (increasing shielding with increasing displacement from equilibrium). A very interesting result is found when the variation of the shielding with respect to the opening of the bond angle is examined in the H_2O, NH_3, and PH_3 molecules, the bond lengths being kept constant. This trace on the shielding surface is concave upward and has its minimum shielding at the tetrahedral angle.[33] Chesnut had reported some calculations in which the bond lengths are continuously optimized while the bond angle is varied. This is of course a more complicated representation in that both bond length and bond angle are changing at once. Nevertheless, he finds that the shielding surfaces are concave upwards and in H_2S the surface is very flat from 90° to 140° in this representation and for PH_3 his minimum also occurs at the tetrahedral angle.[20] The equilibrium angle for H_2O and NH_3 is very close to tetrahedral, whereas for H_2S, H_2Se, and PH_3 it is less than tetrahedral. H_2Se and PH_3 shielding surfaces have a sizeable slope at the equilibrium bond angle.[33,34]

Other molecules have only been studied in terms of the derivatives of the shielding with respect to bond extension at the equilibrium geometry. The first derivatives of the shielding with respect to bond lengthening in the first- and second-row hydrides were calculated by Chesnut.[20] Be in BeH_2, Mg in MgH_2, B in BH_3 and Al in AlH_3, all were found to have positive derivatives. The first derivatives of the non-H nuclear shielding in these

hydrides changed smoothly in going from left to right in the Periodic Table, rising to a maximum at group 2 and dropping to large negative values toward group 7. This smooth change has been explained[23] as we shall find in a later section of this review. A comprehensive survey of first and second derivatives of the shielding for molecules containing first-row atoms by Chesnut and Wright[35] confirmed earlier predictions. In discussing these we make a distinction of primary (with respect to the stretch of the bond to the nucleus in question) and secondary (with respect to the stretch of a remote bond) derivatives:

(1) Most of the primary first derivatives are negative, that is, a nucleus tends to become deshielded upon extension of a bond in which it is involved. In this study, only 13 out of about 270 primary first derivatives were found to be positive. Negative derivatives ranged from -4 to -2784 ppm Å^{-1}. The few positive derivatives ranged from $+0.3$ to $+39.0$ ppm Å^{-1}.

(2) The derivatives with respect to extension of a multiple bond are generally larger than those involving the extension of a single bond.

(3) The shielding derivatives with respect to extension of a bond to hydrogen are generally smaller than those involving extension of bonds to heavy atoms.

(4) The paramagnetic terms dominate the shielding derivatives.

(5) The shielding derivatives of non-hydrogen nuclei tend to parallel the equilibrium isotropic shielding itself, independent of the nuclear species involved, that is, the shielding derivative decreases algebraically as the isotropic shielding of the nucleus decreases, but especially so for multiple bonds. An example is shown in Fig. 3.

It should be noted that all these general trends had already been proposed much earlier by Jameson[36–38] and by Jameson and Osten[39,40] (see Ref. 40 for references) in their interpretation of the very large body of experimental isotope shift data and the temperature dependence of the chemical shifts in the zero-pressure limit of ^{19}F in several molecules and ^{13}C in CO and CO_2, ^{15}N in N_2 and NNO. Indeed it was the general trends in the experimental data that formed the basis for the interpretation. While the rovibrational averaging theory was complete, the experimental data could not be inverted

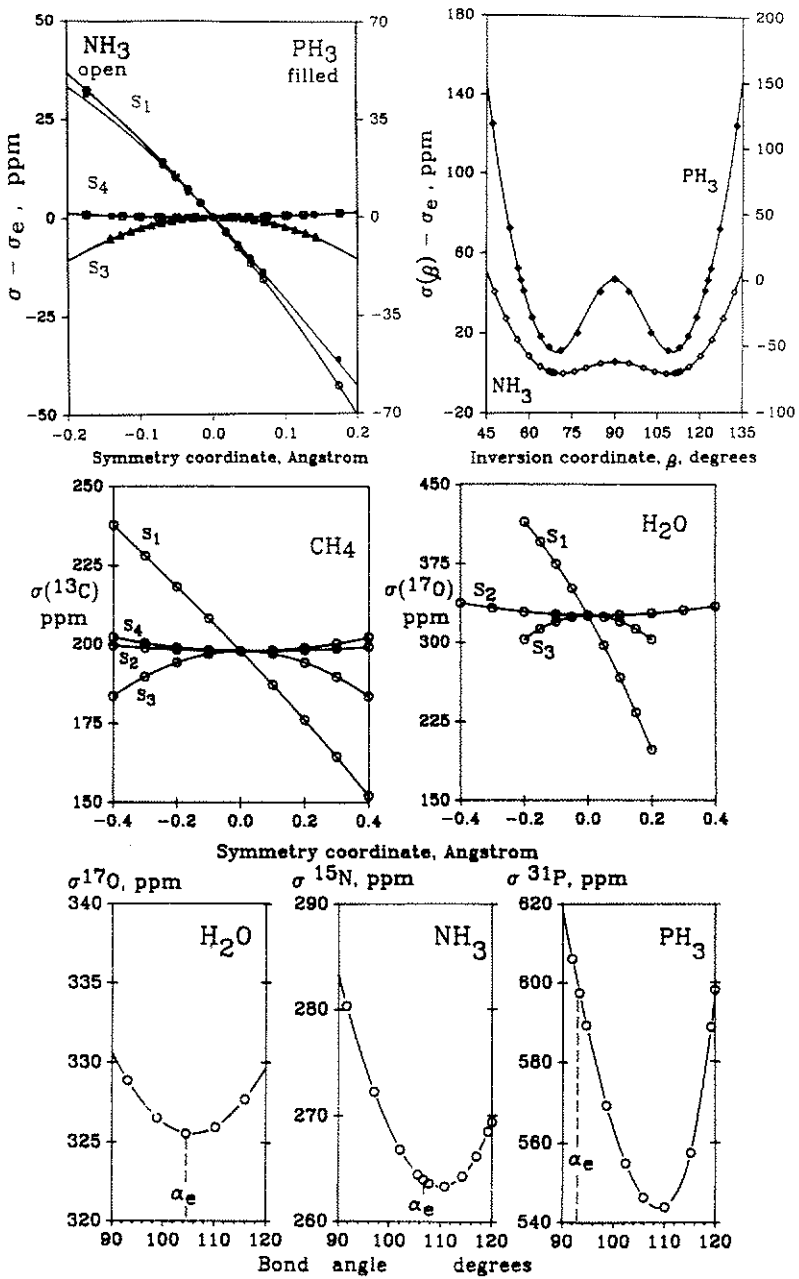

Fig. 2. Traces on the shielding surfaces of ^{17}O in the H_2O molecule,[30] ^{13}C in CH_4,[31] ^{15}N in NH_3,[32] and ^{31}P in PH_3.[33] The symmetry coordinate S_1 is the totally symmetric stretch, S_2 is the symmetric angle deformation or the inversion coordinate (in the case of NH_3 and PH_3). S_3 and S_4 are the asymmetric stretches and angle deformations, respectively.

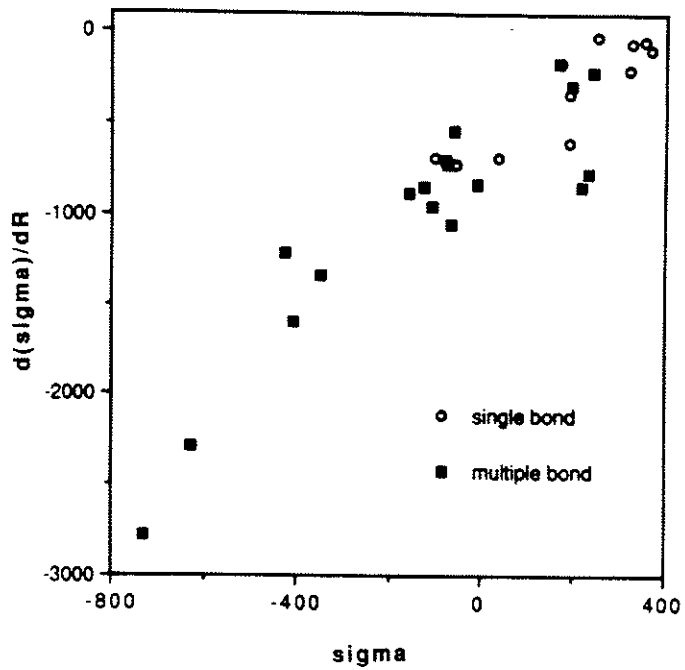

Fig. 3. The first derivatives of the ^{17}O shielding with respect to extension of the bond correlates with the absolute shielding. Reproduced from Ref. 35 with permission of John Wiley & Sons, Inc. Copyright © 1991 John Wiley & Sons, Inc. These are *ab initio* values calculated using the GIAO method.

to provide more than the empirical derivatives $(\partial\sigma^X/\partial r_{AX})_{eq}$. The ability of local origin methods to describe adequately the shielding even with modest basis sets has now made possible the theoretical investigations of these earlier conclusions and to find their limitations and conditions of applicability.[35] Furthermore, Chesnut's survey of shielding derivatives offers new information about second derivatives $(\partial^2\sigma^X/\partial r^2_{AX})_{eq}$. Most of the second derivatives are negative, that is, a nucleus tends to become deshielded upon bond extension in a more pronounced way than linearly. Of the 210 second derivatives, 42 were found to be positive (these involved proton shieldings in most cases). Second derivatives are not small, that is, the trace along the shielding surface corresponding to a symmetric stretch of the bonds is not linear at the point corresponding to the equilibrium geometry of the molecule.

The shielding dependence on bond length has also been examined in model fragments (*N*-formyl-L-amino acid amide) for glycine, alanine and valine residues in proteins.[41] Likewise, in these model compounds, the first

and second derivatives of the C^α chemical shielding with respect to its bond lengths, C^α–N, C^α–C^O, C^α–H^α and C^α–C^β (for alanine and valine) are found to be negative. The magnitudes of these derivatives were sufficiently large (40–90 ppm $Å^{-1}$) to permit an evaluation of the spread of bond length values for a particular residue reported in X-ray structures of proteins.[42] After considering the range of chemical shift inequivalencies observed in proteins, it has been deduced that the differences in bond lengths currently reported in X-ray structures are too large to be consistent with NMR data.

An interesting observation that can be made from these studies is the apparent transferability of these shielding derivatives from one amino acid to another. Both alanine and valine have very similar first derivatives for the shielding of C^α with respect to the C^α–N stretch (Ala; −88 ppm $Å^{-1}$, Val; −84 ppm $Å^{-1}$), C^α–C^O(Ala; −57 ppm $Å^{-1}$, Val; −60 ppm $Å^{-1}$), and C^α–C^β (Ala; −16 ppm $Å^{-1}$, Val; −17 ppm $Å^{-1}$). On the other hand, even though glycine lacks C^β, its derivatives are not too far from alanine and valine: C^α–N (−69 ppm $Å^{-1}$) and C^α–C^O(−48 ppm $Å^{-1}$). The glycine derivatives being numerically 80% of the alanine and valine derivatives may reflect in the ground-state vibrational corrections as pointed out by Laws *et al.*[42]

The corresponding C^β shielding derivatives also show some interesting characteristics. First of all, the first derivatives of C^β shielding with respect to the bond lengths C^α–N and C^α–C^O were found to be positive in sign.[41] On the other hand, its derivative with respect to C^α–H^α is still negative but an order of magnitude smaller (−7 ppm $Å^{-1}$ for C^β compared to −57 ppm $Å^{-1}$ for C^α). The dependence of the C^β shielding on the bond length C^α–C^β appears to be normal. It is noteworthy, however, that the two model fragments, alanine and valine, differ greatly in magnitude in terms of this shielding derivative. Alanine has −36 ppm $Å^{-1}$ for $\partial\sigma^{C^\beta}/\partial r(C^\alpha\text{–}C^\beta)$ while valine has −69 ppm $Å^{-1}$, nearly twice the value for alanine. This difference indicates that the presence of methyl groups on C^β in valine leads to a greater sensitivity of the C^β shielding to the C^α–C^β bond length. This is consistent with the well-known incremental effects of methyl substitution in deuterium-induced isotope shifts.

The dependence of shielding on bond angle as seen in small molecules is much more complicated than its dependence on bond length. In fact, using the first derivative of the shielding with respect to bond length normally would suffice. On the other hand, the shielding as a function of bond angle in Fig. 2 shows definite curvature. And as observed in the small hydrides (Fig. 2), an extremum (minimum shielding) is found near the tetrahedral value. Hence, in order to take into account bond angle influences on shielding, one needs to take into account higher-order derivatives. The same trends are seen in model fragments for amino acid residues in proteins. Glycine, for example, shows a minimum for the C^α shielding when the N–C^α–C^O angle is close to the tetrahedral value,[41] the surprising feature

seen in small hydrides.[33] Alanine and valine also show a minimum, although at a smaller value of this angle.

Since the shielding derivatives with respect to bond angle changes are smaller in absolute terms compared to bond length derivatives, the experimental verification of the bond angle dependence of shielding is more difficult. It is unlikely for observed shielding changes to be dominated by bond angle contributions. The temperature dependence of the ^{15}N shielding in ammonia is indeed a rare case. In this molecule, it is the large-amplitude inversion motion that makes bond angle contributions to the observed temperature dependence significant.

2.1.3. Dihedral angle

In addition to the previously discussed bond length and bond angle dependencies, the chemical shielding also exhibits sensitivity to torsion angles. For example, the phenomenon called the γ-gauche effect, first discovered by Paul and Grant[43] in hydrocarbons, indicates that ^{13}C nuclei at γ-positions are ~5 ppm more shielded in a *gauche* than in a *trans* conformation. Moreover, Anet and Cheng[44] have also demonstrated that the α- and β-positions are likewise deshielded in the *trans* conformation. Recently, Webb and coworkers[45] have attempted to explain the observed γ-gauche effect using *n*-octane as a model compound. Their results indicated that the γ-position is indeed more shielded in the *gauche*-conformation, about 3 ppm compared to the *trans*-conformer. It is important to note that in these calculations, the bond lengths and bond angles were relaxed at each torsion angle. Hence, the changes in shielding may not be direct consequences of variations in the torsion angle. Prior to Webb's work, there have been a number of previous studies on how dihedral angles influence shielding. The simplest case of ^{13}C shielding dependence on dihedral angles is found in ethane where Chesnut *et al.*[46] have shown using the GIAO method that the ^{13}C nuclei in the eclipsed conformation are 4.66 ppm more shielded than in the staggered conformation. Geometry optimizations were also performed at each dihedral angle. Using calculated shielding derivatives with respect to bond length and bond angle changes and knowing how much these geometrical parameters had changed upon minimization, they were able to extract the change in shielding that can be directly attributed to the torsion angle variation. They arrived at the conclusion that nearly 90% of the change in shielding is due to torsion angle effect alone. IGLO calculations on ethane as reported by Kutzelnigg *et al.*[47] agree favourably with Chesnut's results. As in the earlier work, the contributions from relaxing the other geometrical parameters are also found to be very small. Barfield and coworkers have studied the influence of the torsion angle in a variety of hydrocarbons.[48,49] In these investigations, geometry optimizations were also employed making it difficult to assign how much of the change in shielding was directly caused by altering the dihedral angle. Geometry optimizations, in addition to being time-consuming, preclude a more specific analysis of torsion angle influences on shielding. Oldfield *et al.*[41,50,51] have generated shielding traces and surfaces that map only the changes in shielding that are a direct consequence of a change in a given torsion angle in a series of compounds ranging from small hydrocarbons to peptide models like *N*-formyl-L-valine amide. These shielding surfaces, besides being free from geometry relaxation effects, surprisingly have been found to be sufficient in explaining ^{13}C chemical shifts in proteins.[51] The torsion angle dependence of shielding in small molecules is difficult to extract: it normally manifests itself in the temperature dependence of the chemical shift along with equally significant contributions from centrifugal distortion. In addition, a change in a dihedral angle manifests itself strongly in the overall shape of a small molecule thereby inducing additional effects from the environment. On the other hand, proteins serve as excellent systems for studying the torsion angle effects on chemical shifts for several reasons. Variable temperature studies are not necessary because a protein already provides sites that differ from each other primarily in torsion angles. Second, a protein being a large molecule assumes an overall shape which is not contingent on one particular torsion angle.

Focusing on the shielding of the nuclei at the α- and β-positions with respect to the dihedral angle of interest, interesting trends are apparent.[50] For small compounds that can be regarded as substituted ethane molecules, substitution at C^α causes a much larger change in the dihedral angle effects on C^β than on C^α shielding. χ^1 denotes the dihedral angle defined by H^α–C^α–C^β–H^β. For example, in the series of hydrocarbons: ethane, propane and 2-methylpropane, as shown in Fig. 4A, the C^α shieldings as functions of χ^1 are very similar. On the other hand, it is obvious from Fig. 4B that the sensitivity of the C^β shielding to χ^1 diminishes with methyl substitution at C^α. A similar situation exists when one introduces functional groups like –C = O and $-NH_2$ on the C^α site.[50] The amino group is found to reduce significantly the sensitivity of the C^β shielding on the torsion angle while the C^α shielding function remains similar to that of the hydrocarbons. In proteins, if one can regard the amino acid residues as substituted ethanes, the presence of amide groups introduces two additional torsion angles that can influence the shieldings of C^α and C^β. These torsion angles are $\phi({}_{i-1}C^O{-}_iN{-}_iC^\alpha{-}_iC^O)$ and $\psi({}_iN{-}_iC^\alpha{-}_iC^O{-}_{i+1}N)$. In Fig. 5, the χ^1 dependence of the shielding in C^α and C^β sites of *N*-formyl-L-alanine amide at various ϕ and ψ angles is shown. The C^α shielding as a function of χ^1 does not seem to change shape with variations in ϕ and ψ as shown in Fig. 5A. On the other hand, C^β (Fig. 5B) behaves differently. First of all, its shielding is less sensitive to changes in χ^1. It no longer resembles the shape of the potential function, the eclipsed conformation (0°) does not exhibit a maximum value for C^β shielding. In fact, when the torsion angle ϕ is

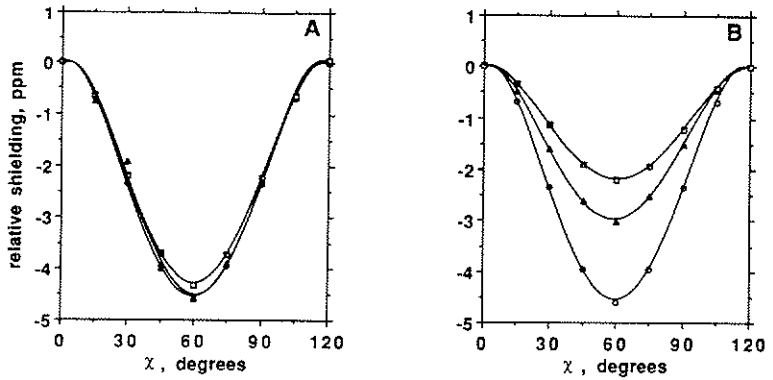

Fig. 4. Calculated ^{13}C shieldings as a function of the torsion angle, $\chi(H_1-C_1-C_2-H_2)$, with increasing methylation. (A) C_2 (C^α) shielding of ethane (○), propane (△), and isobutane (□). (B) as in (A) but for (methyl) C_1 (C^β). Reproduced from Ref. 50, with permission. Copyright 1993, American Chemical Society.

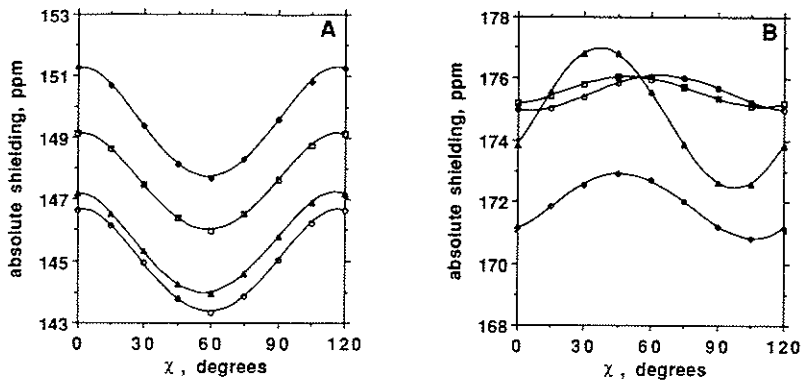

Fig. 5. Calculated ^{13}C shieldings as a function of the torsion angle, χ, for an alanine model fragment, at various ϕ and ψ angles. (A) C^α shielding for helix ($\phi = -58$, $\psi = -51$) (○), turn ($\phi = 55$, $\psi = 50$) (△), sheet 1 ($\phi = -140$, $\psi = 140$) (◇), and sheet2 ($\phi = -71$, $\psi = 140$) (□). (B) as in (A) but for (methyl) C^β. Reproduced from Ref. 50, with permission. Copyright 1993, American Chemical Society.

positive, the shielding function also loses a relative extremum at the staggered conformation (60°). Interestingly, positive ϕ angles correspond to conformations in which C^β is close to C^O. Secondly, the χ^1 dependence of the C^β shielding varies with ϕ and ψ. What is clear in both C^α and C^β pictures, however, is that the shielding inequivalencies observed between sheet and helical residues are dominated by ϕ and ψ effects. Since the range

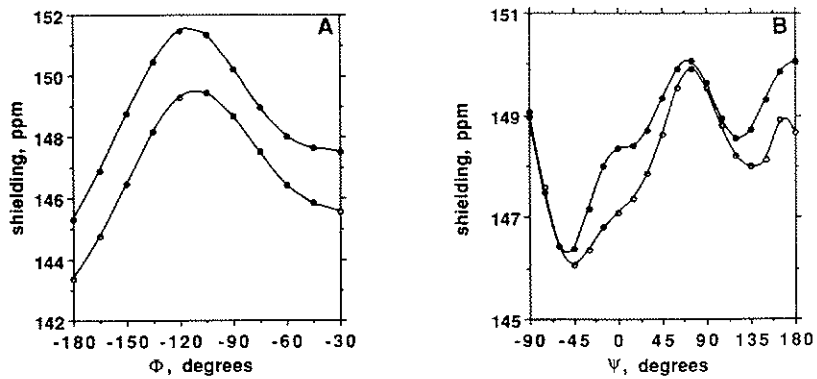

Fig. 6. (A) Calculated C^α shielding for an alanine model fragment as a function of the torsion angle ϕ, at different ψ angles: $\psi = 60$ (○) and 135 (●). (B) as in (A) but as a function of ψ, at different ϕ angles: $\phi = -60$ (○) and -150 (●).

of ϕ and ψ values normally observed in proteins is large, traces with respect to one torsion angle on the shielding surface are not sufficient. To demonstrate this, Fig. 6 shows how the shielding function with respect to one torsion angle changes when one varies the other torsion angle. Although ϕ and ψ describe rotation about a bond that consists not only of sp^3-hybridized C as in χ^1 but also N (in ϕ) and C^O (in ψ), resemblances to the χ^1 dependence seen in hydrocarbons are present. For example, conformations in which bulky groups are close to each other result in greater shielding while staggered conformations are deshielded. Figure 6A shows the dependence of C^α shielding on the torsion angle ϕ at fixed values of $\psi\{-60°(○)$ and $135°(●)\}$. The curves are almost parallel to each other indicating that separating the ϕ effects from ψ contributions is possible. However, in Fig. 6B, it can be seen that this observation is caused by a fortuitous choice of ψ angles in Fig. 6A. Although the curves still exhibit similar shapes, their separation is clearly not constant within the range of ψ angles shown. The ψ dependence clearly changes with variations in ϕ. Thus, it can be deduced from this figure that the C^α shielding equivalencies arise from a combination of ϕ and ψ effects and, apparently, do not lend themselves to separability. Surfaces are therefore needed to describe how ϕ and ψ influence chemical shielding in proteins. Figure 7 shows a ϕ–ψ shielding surface for the model alanine compound.[41,51]

For the valine model compound, *N*-formyl-L-valine amide, the presence of substituents at the C^β site not only reduces the symmetry but also induces a larger χ^1 dependence for the shielding of both C^α and C^β nuclei. These expected characteristics are certainly observed, as shown in Fig. 8. In valine the staggered conformations at $\chi^1 = 60°$, $-60°$ and 180° are unique

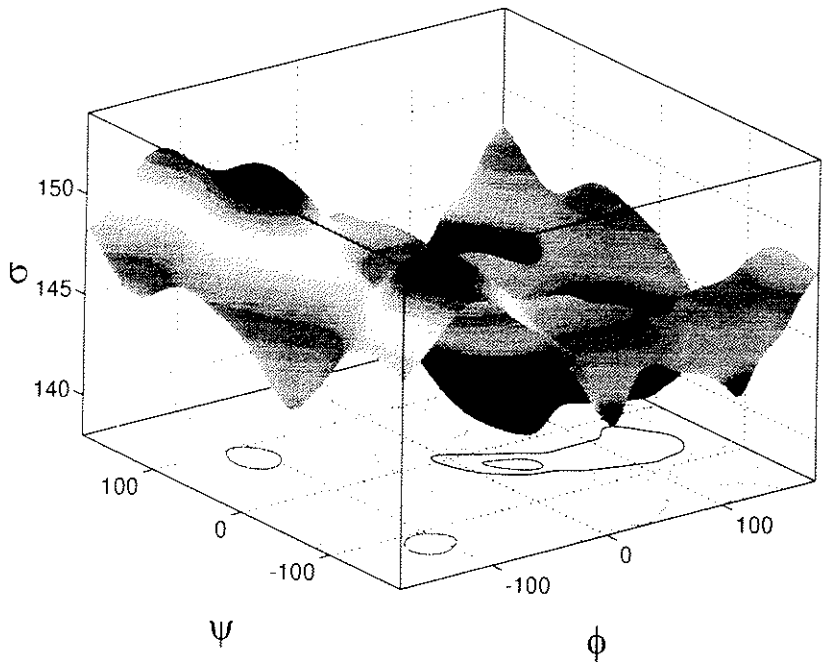

Fig. 7. The C^{α} shielding for an alanine model fragment as a function of the torsion angles ϕ and ψ. Reproduced from Ref. 51.

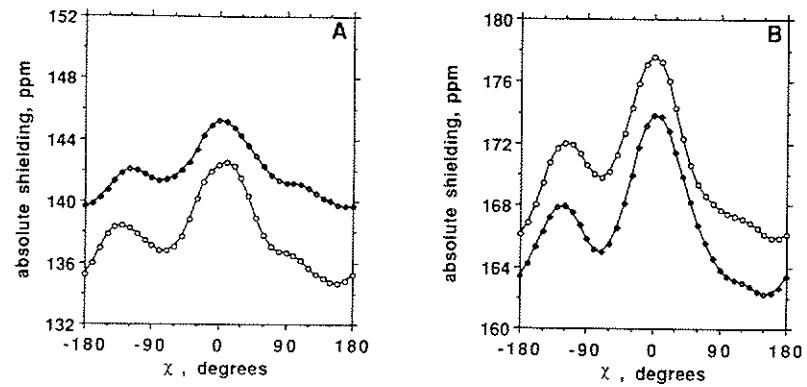

Fig. 8. Calculated ^{13}C shieldings as a function of the torsion angle, χ^1, for a valine model fragment, at different ϕ and ψ angles. (A) C^{α} shielding for helix ($\phi = -55$, $\psi = -55$) (○) and sheet (f = −136, $\psi = 143$) (◇). (B) as in (A) but for C^{β}. Reproduced from Ref. 50, with permission. Copyright 1993, American Chemical Society.

conformations. The *trans*-conformer is clearly deshielded compared to the *gauche*-conformers for both C^{α} and C^{β} whether the compound has sheet-like (◇) or helical (○) ϕ and ψ angles. Consequently, in order to describe the chemical shift equivalencies observed for C^{α} and C^{β} in valine sites in proteins, one needs to take into account not only ϕ and ψ effects but χ^1 as well. Thus, in the most recent work of de Dios and Oldfield,[50] ϕ–ψ shielding surfaces for both C^{α} and C^{β} in *N*-formyl-L-valine amide were reported at each of the staggered conformations, and these are shown in Fig. 9. As a dramatic demonstration of the usefulness of these surfaces, the side-chain conformations of valine sites in the protein Calmodulin have been determined successfully.[50] Effects of the torsion angles ϕ, ψ and χ^1 are not exclusive to C^{α} and C^{β} chemical shifts. It has been shown that ^{15}N likewise shows dependence on these dihedral angles.[52,53] For ^{15}N sites in valine residues, the sensitivity of ^{15}N shielding to the torsion angle χ^1 has been demonstrated using a model valine fragment;[52] a range of at least 10 ppm is predicted for the ^{15}N chemical shift for the three staggered conformations. Empirical studies[53] also show that ^{15}N chemical shifts in proteins are strongly influenced by ϕ and ψ_{i-1} (the ψ angle of the preceding residue).

The differences in side-chains of the various amino acids result in a need for individual shielding surfaces. A generalized ϕ–ψ chemical shift surface obtained empirically is already available[54] but the applicability of such a surface is now in question after seeing that χ^1 effects in valine can contribute as much as 4 ppm. Theoretical shielding surfaces offer several advantages over empirical ones. First, one is not limited to the range of ϕ and ψ angles that has been observed in proteins. Second, the shielding changes due solely to torsion angle changes can be obtained from theory directly. Lastly, each amino acid is treated separately. Although the building of theoretical shielding surfaces is an enormous task, this is certainly feasible with the computer resources presently available.

2.1.4. Remote bond extension

It had been suggested that chemical shifts due to isotopic substitution at positions two or more bonds away from the resonant nucleus could be attributed predominantly to the change in dynamic averaging at the substitution site coupled with the shielding derivative with respect to the remote bond extension.[55,56] Chesnut and Wright found that these so-called secondary derivatives for molecules containing atoms in the first row of the Periodic Table are not always smaller than the primary first derivatives.[35] That is, it can happen that the shielding of a nucleus is changed more substantially by the stretch of a remote bond (especially a multiple bond) than by the stretch of a bond in which it is a participant. The general observation is that the secondary first derivatives in nearly half the cases are comparable to or greater in magnitude than their associated primary

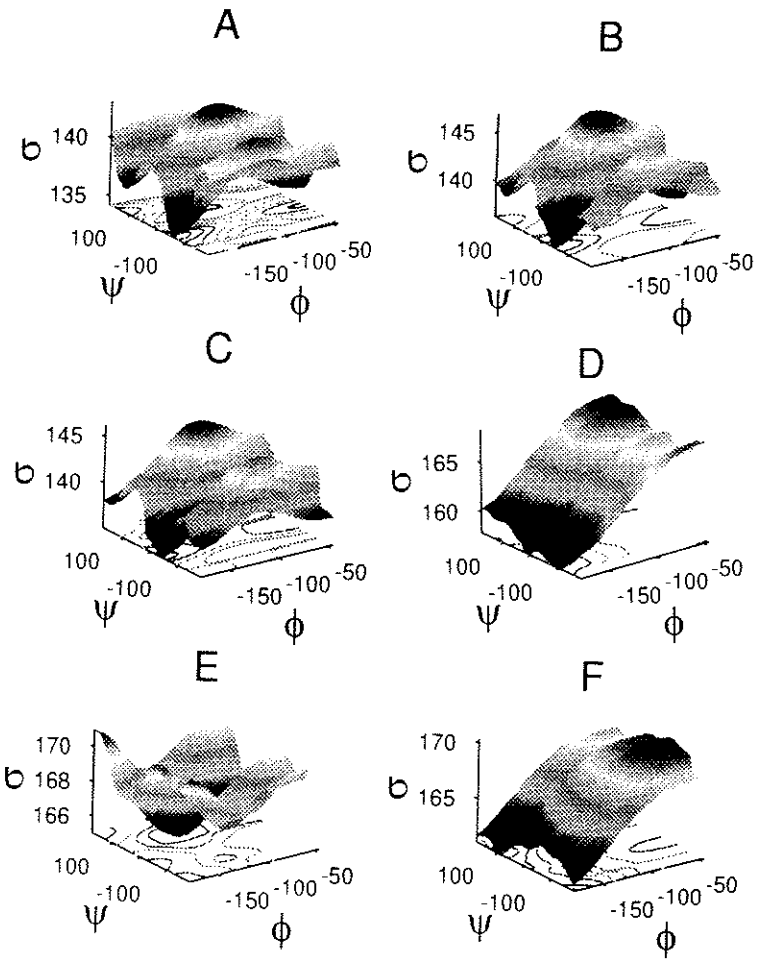

Fig. 9. The C^{α} and C^{β} shielding for a valine model fragment as a function of the torsion angles ϕ and ψ (at various χ^1 values). (A), C^{α}, $\chi^1 = 180°$, (B) C^{α}, $\chi^1 = 60°$, (C) C^{α}, $\chi^1 = -60°$, (D) C^{β}, $\chi^1 = 180°$, (E) C^{β}, $\chi^1 = 60°$, and (F) C^{β}, $\chi^1 = -60°$. Reproduced from Ref. 50, with permission. Copyright 1993, American Chemical Society.

derivatives. A corollary to this is the finding that modification of a remote single bond is not propogated as efficiently in the molecular framework as is modifying a multiple bond.

2.2. Intermolecular shielding surfaces

The intermolecular shielding function is obtained by a supermolecule calculation involving the cluster of two or more interacting molecules as a function of the distances and orientations of the monomers. The intermolecular part of the shielding is then obtained by subtracting out the monomer contributions which have been calculated separately at each configuration by including counterpoise corrections. The latter are necessary in order to take into account the much larger basis set in which the cluster calculations are carried out, and a usual type of approach is to use the full set of orbitals, including the ghost orbitals (without the atoms) centered at the positions of the interaction partners.[57] Intermolecular shielding surfaces prior to 1993 have been reviewed.[13]

2.2.1. Distance dependence

It had been suggested, in an attempted inversion of the experimental second virial coefficient of the Xe shielding in pure xenon gas that the shape of the intramolecular shielding function for two interacting rare gas atoms is similar to the shape of the H_2^+ intramolecular shielding surface, having a minimum in the shielding at some internuclear separation close to the minimum of the potential energy surface.[58] However, previous theoretical calculations exhibited a positive shielding in this vicinity, which would have given rise to a density dependence of opposite sign to that universally observed. The first theoretical indication of a minimum in the intermolecular shielding was obtained by Grayce and Harris who calculated the prototypical intermolecular shielding function, that is, the intermolecular shielding surface of the triplet state of the H_2 molecule, by a truly gauge-invariant density functional method using an electron gas approximation.[59] The very early calculation by Marshall and Pople for the same system using a minimal basis set did not exhibit such a minimum.[60] Owing to the approximate nature of these calculations, the definitive shape of the intermolecular shielding function was not established until the LORG and SOLO calculations of the ^{39}Ar shielding in the interacting Ar–Ar system by Jameson and de Dios.[24] Figure 1 shows this surface. Subsequently, the ^{39}Ar shielding in Ar–Ne, the Ne shielding in Ne–Ne and Ne–He[23] (shown in Fig. 10) and the He shielding in the He–He system[47] were reported. The latter exhibited a minimum only at the correlated level of calculation (MC-IGLO) whereas the correlation contributions to the ^{39}Ar shielding in the Ar–Ar system had

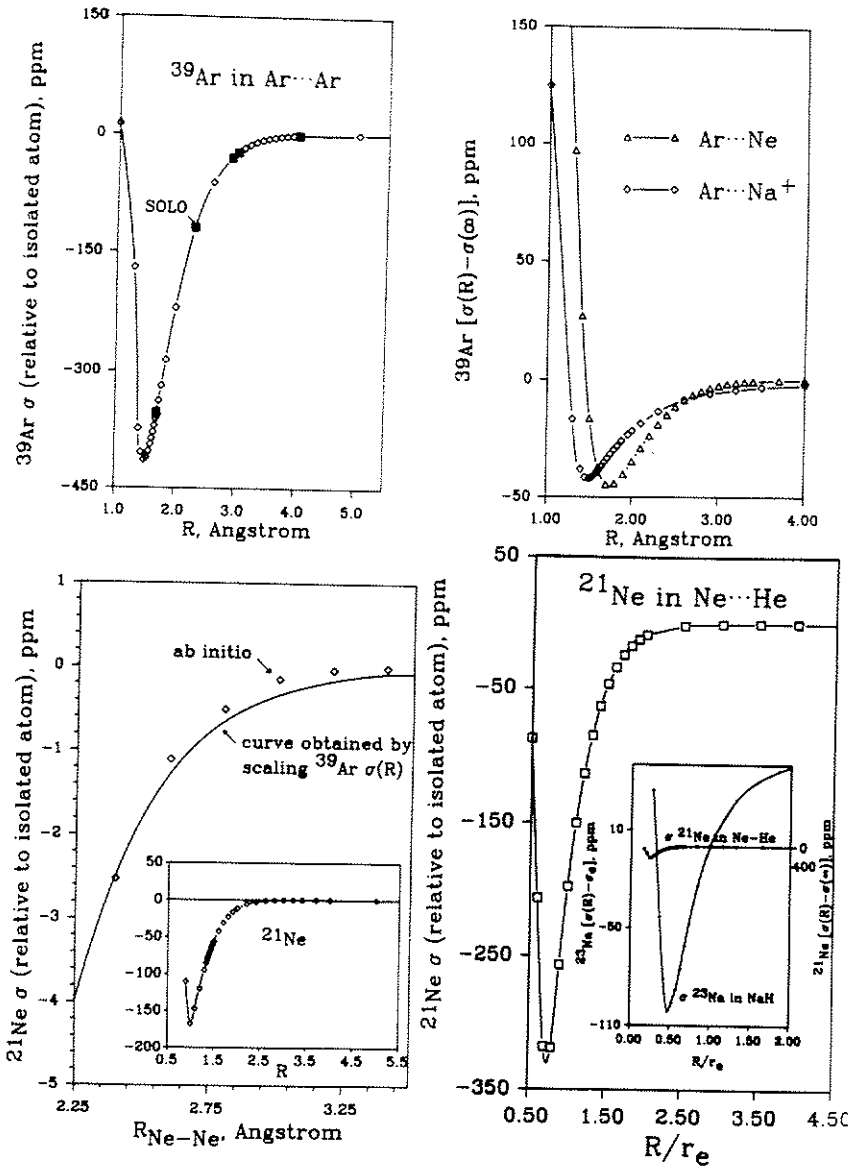

Fig. 10. Intermolecular shielding surfaces for ^{39}Ar in Ar–Ne, ^{21}Ne in Ne-Ne, and ^{21}Ne in Ne-He. Reproduced from Ref. 23, with permission. The ^{39} Ar in Ar-Ar surface scaled down to ^{21}Ne in Ne–Ne agrees reasonably well with the *ab initio* Ne–Ne surface. The magnitude of the intermolecular shielding in the Ne–He system is compared with that of the intramolecular ^{23}Na surface in the isoelectronic NaH molecule by scaling the vertical axes according to $<a_0^3/r^3>$ of ^{21}Ne and ^{23}Na.

been shown by SOLO calculations to be negligibly small. In all rare gas pairs the minimum in the shielding surface occurs at a distance that is well inside r_0, the separation at which the potential energy of interaction goes to zero. An interesting result which was found in comparing common-origin CHF calculations with local origin LORG calculations for the shielding in Ar_2 is that the common origin CHF results show an artefactual positive hump in the region of interest whereas the local origin calculations give only negative intermolecular shielding in this region. The earlier CHF calculations for proton and He shielding in the H_2–He system[61] do show the same positive hump, leading us to believe that this behaviour is an artefact of the gauge problems associated with common-origin calculations using modestly large basis sets. The dependence on the internuclear separation in those regions where sampling at ordinary temperatures would occur for ^{39}Ar shielding is $R^{-6.67}$ for Ar–Ar, $R^{-6.79}$ for Ar-Ne, and for ^{21}Ne shielding it is $R^{-6.74}$ for Ne-Ne, $R^{-7.41}$ for Ne–He.[23]

2.2.2. *Scaling of intermolecular shielding*

It is well known that the sensitivity of the chemical shifts to changes in chemical environment scale according to the characteristic $<a_0^3/r^3>$ of the free atom in its ground state, clearly demonstrated by the correlation of the ranges of the chemical shifts of the nuclei with this quantity.[62,63] We therefore expect the intermolecular shielding function to scale approximately according to this atomic property. Furthermore, to the extent that the intermolecular shielding is effected by the distortion of the electron charge distribution of the atom in response to the presence of the other atom, the magnitude of the effect could be related to the usual quantities that appear in the London model for dispersion energy. It is found that the shapes of the intermolecular shielding surfaces for rare gas pairs are very similar, and the nearly identical R dependence at separations around or larger than r_0 suggests that they may be conformal in the same sense that the law of corresponding states suggests that potential energy surfaces are conformal.[24] It has been found that the rare gas intermolecular shielding functions do scale according to factors that have to do with the sensitivity of the nuclear shielding to the presence of a neighbour. The suggested factors for the shielding of 1 due to the presence of 2 are:

$$\alpha_1<a_0^3/r^3>_1\alpha_2 U_1U_2/(U_1+U_2),$$

where α_1 is the electric dipole polarizability of the rare gas atom in question and $<a_0^3/r^3>_1$ is characteristic of the atom in its ground state, which is a well-known measure of the sensitivity of nuclear shielding,[62,63] and U_1 is the first ionization potential of the atom. These scaling factors have been tested in several ways. First, the shielding function from the scaled ^{39}Ar in Ar–Ar

was compared to the *ab initio* shielding function of ^{21}Ne in Ne–Ne in the region of interest.[24] This produced curves that were nearly superposable in the range of distances of interest, as shown in Fig. 10. Second, the ^{39}Ar shielding in Ar–Ar, scaled to the ^{129}Xe shielding in Xe–Ar, Xe–Kr, and Xe–Xe, produced intermolecular shielding curves for ^{129}Xe which provided excellent agreement with experiment when used to calculate the magnitudes and temperature dependence of the second virial coefficient of the ^{129}Xe nuclear shielding in the rare gas mixtures.[24]

2.2.3 *Additivity and non-additivity*

The additivity of intermolecular shielding has been tested in polar and non-polar systems. In the simplest case, the ^{39}Ar shielding in the presence of two neighbour Ar atoms in the Ar_3 cluster in the form of an equilateral triangle and also in the ^{39}Ar in linear symmetrical Ar_3, can be compared with the ^{39}Ar shielding with only one neighbour in Ar_2. It is found that in the region where the internuclear distances are close to or larger than r_0 of the Ar_2 potential, the intermolecular shielding function for the central ^{39}Ar in the linear trimer and the Ar in the triangular trimer are nearly exactly superposable with 2.0 times the intermolecular shielding function of Ar in the dimer.[24] Therefore, except at close distances that are sampled only at very high temperatures or pressures, the intermolecular shielding of rare gas atoms are additive. It is this additivity that can be called upon to provide interpretation of the ^{129}Xe chemical shifts in the clusters Xe_1, Xe_2, Xe_3, . . ., Xe_8 trapped in the alpha cages of zeolite NaA.[64]

In another example involving larger systems, the solvation shifts due to one HF up to five HF molecules at specific sites around the ^{19}F of the fluorobenzene molecule have been calculated. It is found that the solvation shifts due to two up to five HF molecules are reproduced by a sum of the individual solvation shifts.[65]

2.2.4. *Hydrogen bonding*

The changes of shielding upon formation of hydrogen bonds have been used empirically as a diagnostic tool. The water dimer serves as an example of the shielding changes in the donor and the acceptor molecules.[66–68] In a calculation using the GIAO approach and ice geometry, and using counterpoise corrections, the shielding changes (ppm) are as shown below:[67]

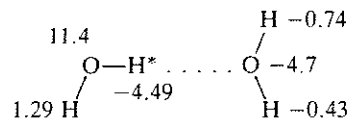

The nuclei of the molecule that donates the proton become more shielded. The nuclei of the molecule that accepts the proton become deshielded, as does the donated proton H*. The shielding changes in the donor molecule are larger than the corresponding changes in the acceptor molecule, the most profound change occurring in the donated proton. Even more drastic is the change in the anisotropy of the proton. In ice, where every proton is involved in a hydrogen bond, it is not sufficient to do a dimer calculation to reproduce the large anisotropy of the proton shielding. For this system, it is found that both the first and the second solvation shells contribute. A calculation on the $(H_2O)_{17}$ cluster in the ice geometry leads to the proton shielding tensor components 11.97, 12.19, 46.91 ppm, with an anisotropy of 34.8 ppm.[69] This is in excellent agreement with the experimental data of Pines *et al.* at 183 K,[70] which when converted to absolute shielding are 12.4, 12.4, 46.4 ppm, with an anisotropy of 34 ± 2 ppm. The calculated anisotropy of the proton shielding in an isolated water molecule is only 15.7 ppm. The profound effect of hydrogen bonding on the anisotropy of the proton was well known experimentally, but was calculated successfully only recently.

The shielding surface was not calculated in the above examples. In the hydrogen bonding situation in the aqueous NH_4^+ ion, modeled by the clusters $NH_4^+(H_2O)$ and $NH_4^+(H_2O)_4$, the shielding surfaces for the N nucleus, for the donated proton (H*), and for the spectator protons attached to the N have been calculated by Munch *et al.*[71] The shieldings change monotonically with N· · · ·O distance. On the other hand, for a fixed N· · · ·O distance, shown in Fig. 11, both the H* shielding and the N shielding change with N–H* distance in a non-monotonic way, exhibiting a minimum. At the typical hydrogen-bonded geometry, the N shielding surface has a negative slope with increasing N–H* distance, as it does in the isolated NH_4^+ ion. The H* shielding surface has a negative slope at this same distance, just like the H shielding in the isolated NH_4^+ ion, but the spectator H shielding surface has a positive slope. It is the latter that is thought to be responsible for the unusual sign of the isotope shift on the protons in $NH_nD_{4-n}^+$ ion. The shapes of these surfaces may be more general. The opposite signs of the slopes of the ^{1}H shielding surfaces of the spectator proton compared to the hydrogen-bonded H* for changes in the N· · ·H* distance may also be the basis for the *D*-induced proton isotope shifts in the hydrogen-bonded sugars, where the H* has a usual sign isotope shift upon deuteration at the acceptor oxygen, whereas the spectator proton on the acceptor has an unusual sign isotope shift upon deuteration of the H*.[72]

The increased shielding of the atom which donates its attached proton to a hydrogen bond is typical. Even in internal hydrogen bonding, such as in phenols, it has been found that the ^{17}O shielding increases upon formation of an internal hydrogen bond.[73] In contrast, using model fragments for a dipeptide, Chesnut and Phung[74] and de Dios *et al.*[52] found that the shielding of an amide N, although much less sensitive to hydrogen bonding compared to O, decreased.

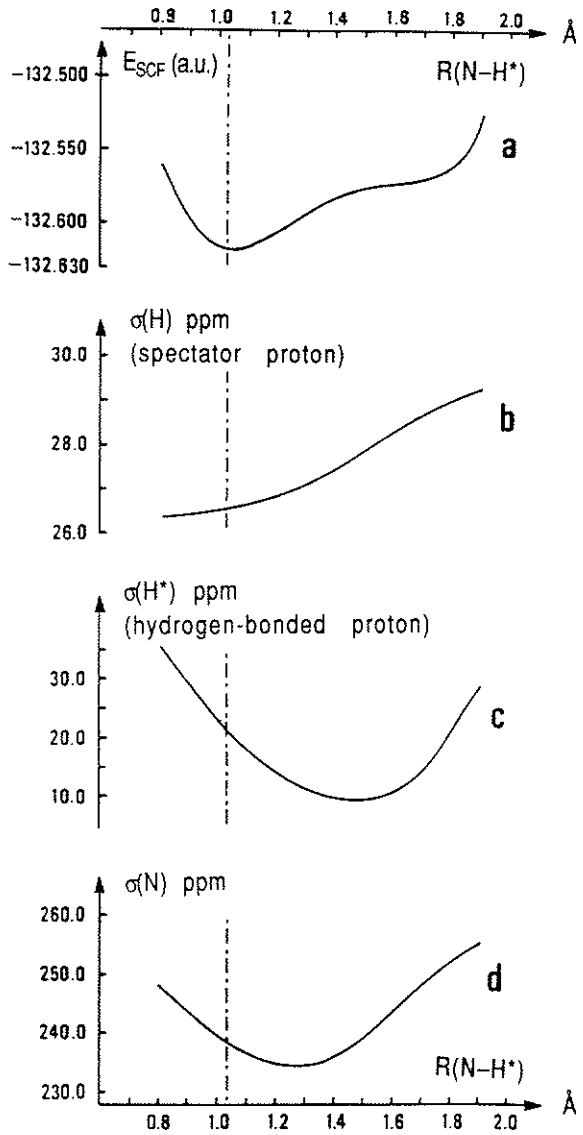

Fig. 11. Shielding surfaces in a hydrogen-bonded system NH_4^+–OH_2. Reproduced from Ref. 71, with permission from *Acta Chemica Scandinavica* (a) The potential energy surface for a fixed N–O distance, varying the position of the H* along the N–O internuclear line (the x axis gives the N–H* separation). (b) The shielding surface of the spectator proton attached to the N. (c) The shielding surface of the hydrogen bonded proton H*. (d) The N shielding surface. The experimental optimum N–H* separation is marked.

2.3. Electric field effects and dispersion contributions

The idea that observed changes in nuclear shielding could be explained in part by the effects of electric fields generated intermolecularly or intramolecularly was proposed by Stephen[75] and Buckingham.[76] The shielding of a nucleus in a molecule in the presence of a uniform electric field **F** was expressed by Buckingham as follows:

$$\sigma_{\alpha\beta} = \sigma_{\alpha\beta}^{(0)} + \sigma_{\alpha\beta\gamma}^{(1)} F_\gamma + \sigma_{\alpha\beta\gamma\delta}^{(2)} F_\gamma F_\delta \tag{1}$$

where the field-independent tensor components $\sigma_{\alpha\beta\gamma}^{(1)}$ and $\sigma_{\alpha\beta\gamma\delta}^{(2)}$ have a number of non-zero independent values depending on the nuclear site symmetry.[77,78] For example, for a $C_{\infty v}$ site, the electric field dependence of the shielding is

$$\sigma_{xx} = \sigma_{xx}^{(0)} + \sigma_{xxz}^{(1)} F_z + (1/2)\sigma_{xxxx}^{(2)} F_x^2 + (1/2)\sigma_{xxzz}^{(2)} F_z^2 + \ldots \tag{2}$$

$$\sigma_{yy} = \sigma_{xx}^{(0)} + \sigma_{xxz}^{(1)} F_z + (1/2)\sigma_{yyxx}^{(2)} F_x^2 + (1/2)\sigma_{xxzz}^{(2)} F_z^2 + \ldots \tag{3}$$

$$\sigma_{zz} = \sigma_{zz}^{(0)} + \sigma_{zzz}^{(1)} F_z + (1/2)\sigma_{zzxx}^{(2)} F_x^2 + (1/2)\sigma_{zzzz}^{(2)} F_z^2 + \ldots \tag{4}$$

It is useful to average all directions of the magnetic field but to leave the molecule fixed relative to the electric field. For a $C_{\infty v}$ site, one then obtains

$$\sigma - \sigma^{(0)} = -AF_{\parallel} - B_{\parallel}F^2 - B_{\perp}F^2 \tag{5}$$

where

$$A = -(1/3)\,[2\sigma_{xxz}^{(1)} + \sigma_{zzz}^{(1)}] \tag{6}$$

$$B_{\parallel} = -(1/6)\,[2\sigma_{xxzz}^{(2)} + \sigma_{zzzz}^{(2)}] \tag{7}$$

$$B_{\perp} = -(1/6)\,[\sigma_{xxxx}^{(2)} + \sigma_{yyxx}^{(2)} + \sigma_{zzxx}^{(2)}] \tag{8}$$

The first-order and second-order electric field coefficients of the shielding have been given the name shielding polarizabilities and hyperpolarizabilities.[79] There are analogous coefficients of the electric field gradients and hypergradients as well.[80,81] The physical picture is as follows: when an electric field is applied along the molecular axis of CO for example, the field induces an electric dipole, which means that charge is shifted along the molecular axis; the charge density will increase at one end of the molecule and decrease at the other end. In a CO molecule oriented such that the electric field is in the O–C direction the field draws charge from C towards O. ^{13}C deshields whereas ^{17}O becomes more shielded. By

symmetry, the signs change when the field direction is reversed. It is very important to have the same definition of the axis system (the positive direction of the z axis) used in the computations when comparing calculations in different molecules and especially when comparing calculations by different authors. As might be expected in a linear molecule, the larger effect is in the shielding tensor component perpendicular to the molecular axis, whereas the purely diamagnetic parallel component exhibits a much smaller change.[82] All the calculations so far reported have involved using a common gauge origin.[79, 81–86] The most important conclusions so far are (a) the shielding polarizabilities are larger for ^{19}F than ^{13}C, and smallest for ^{1}H,[82,87] and (b) that the electric field coefficients are very dependent on the chemical bonding of the nucleus in question. For example, they are roughly an order of magnitude larger for ^{17}O in H_2CO than in CO.[87] For the highly symmetric nuclear sites of ^{13}C in CH_4 and ^{29}Si in SiH_4 only the B term is non-zero and these are found to be of opposite signs, with the ^{29}Si being unusual.[87] These quantities are interesting in their own right as molecular electronic properties. It has been found that the contributions to the shielding due to the second-order terms (hyperpolarizabilities) are rather small,[81,88] contrary to the original contention that the B terms were responsible for most of the large medium effects on Xe chemical shifts and on ^{31}P in P_4. The full *ab initio* calculations on the rare gas pairs have of course already shown that the short range (which might be termed overlap compression and exchange) contributions are large whereas the dispersion contributions are small.[24]

Although the original idea of Raynes, Buckingham and Bernstein[89] to replace the dispersion contributions to the shielding by the effects of fluctuating electric fields[90,91] for which the B term in the uniform electric field calculations can then be applied is no longer sustainable, the distance dependence predicted by a consideration of the electric fields due to a point charge or a permanent electric dipole continues to be useful.[23] By a consideration of the shielding response to a point charge, electric dipole, quadrupole, etc., the proper responses in the long-range limiting situation, it has been possible to understand the distance dependence that has been found in the *ab initio* calculations of ^{39}Ar in the presence of Na^+ ion and NaH molecule.[23] The former has a nearly R^{-4} dependence at large separations whereas the latter has more nearly an R^{-6} dependence.

In the context of this review, however, the importance of these electric field and field gradient terms in the shielding is underscored in the consideration of electrostatic effects of counterions and polar groups. The effects of the very large numbers of water molecules solvating a protein, for example, cannot be taken into account computationally by doing calculations in the presence of realistic water molecules. One approach to the shielding contributions due to distant parts of the protein has been suggested by Oldfield and coworkers:[52] to replace the shielding contributions from distant residues by considering only the classical electric fields and field gradients generated by electrostatic models (AMBER point charges for example) at the nucleus in question coupled with the response of the nuclear shielding to such electric fields and field gradients.

These ideas present two challenges. One is, how well does representing the solvent molecule by a point charge model evoke the appropriate shielding response? Second, how well does the use of the product of the shielding polarizability with the electric field at the nucleus replace this response? The answer to the first question is obtained by comparing two *ab initio* shielding calculations: one is a supermolecule calculation for the solute molecule in the presence of the solvent molecules and the other is for the solute molecule in the presence of the point charge models for the solvent molecules. This comparison has been done for the ^{19}F nucleus in fluorobenzene with various numbers of HF as solvent.[65] In the answer to the second question, comparing results obtained from full *ab initio* computations with those derived from the shielding polarizability approach, it has been evident that in order to reach agreement, terms up to the hypergradient of the field need to be considered.[81] On the other hand, terms arising from the shielding hyperpolarizability can be neglected. However, caution should be exercised in applying such conclusions reached in calculations on rigid static systems to real systems where there is motional averaging. In the presence of motion, it is only expected that the various electric field terms would average differently.

2.4. Is there a global shape for the traces on shielding surfaces?

The similarities found in those shielding surfaces that have been calculated over a fairly wide region of configuration space[13,23,33] offer some hope of being able to transfer some of the insight gained in the few calculations to a more general application to more complex systems. First, it has been noted that the intramolecular shielding surfaces of the small molecules H_2O, CH_4, NH_3, and PH_3 have shapes in common with respect to the shielding dependence on the nuclear displacement coordinates such as the symmetry coordinates of the molecule.[33] Then, it was suggested that the intramolecular shielding surfaces in terms of the changes in shielding upon bond extension of diatomic molecules related in the Periodic Table can be scaled to one another, at least in the vicinity of the equilibrium geometry, by use of the factors $R_e\langle a_0^3/r^3\rangle$.[23] The suggested global characteristics of shielding functions are analogous to the global shape of diatomic molecule potential functions in the vicinity of the equilibrium geometry and the relationships between the Morse parameters associated with bond stretching.[92] Third, it has been noted that the intermolecular shielding functions for rare gases have fairly similar R-dependence in the interesting region of internuclear

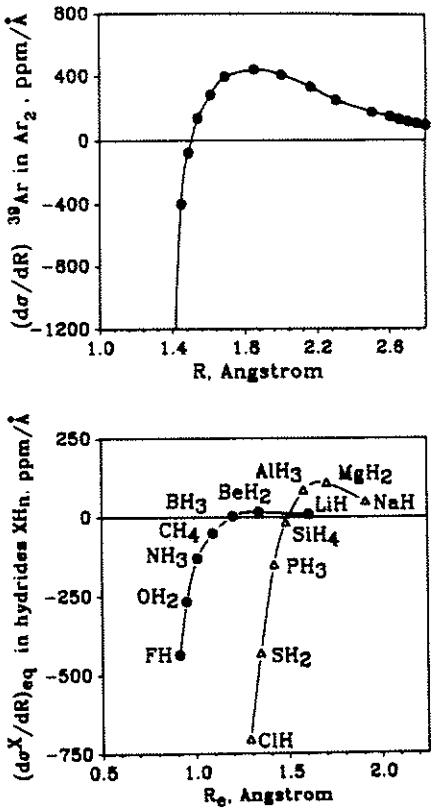

Fig. 12. The upper figure is the derivative of the ^{39}Ar shielding surface in Ar–Ar as a function of the internuclear separation. Below are the derivatives of the X shielding surface at the equilibrium geometries of the hydrides XH_n, plotted against their experimental equilibrium X–H bond lengths. Reproduced from Ref. 23, with permission.

separations, having R^{-n} shapes at large R, when n ranges from -6.6 to -7.4, and the shielding functions at these separations were found to scale by factors that are related to the susceptibility of the rare gas atom to a distortion away from spherical symmetry in the presence of a neighbour atom and the sensitivity of the shielding to such distortions,[23] already mentioned in Section 2.2.2. Fourth, the similarity in the overall shape of the intermolecular shielding surface to the intramolecular shielding surface of one of the nuclei in a diatomic molecule has been discussed,[23] and exhibited in Fig. 1. Fifth, the variation in the derivatives of the X shielding surfaces of the hydrides XH_n of the first and second rows of the Periodic Table has been found to be easily understood in terms of a natural progression in the

equilibrium X–H bond length in going from left to right in the Periodic Table, thereby providing a systematic progression in the derivative of the shielding in that part of the shielding surface that is at the equilibrium bond length, as can be seen in Fig. 12. Thus, the systematic algebraic change from the positive (unusual sign) shielding derivatives with respect to the bond stretch for the alkali and alkaline earth hydrides to the large negative derivatives for the hydrogen halides can be viewed as a natural consequence of a systematic progression from one part of the same-shape shielding surface to another. The preponderance of the negative first derivatives of shielding with respect to bond stretching is then merely a consequence of the scarcity of experimental data in the nuclei of groups 1–3 of the Periodic Table. The results of the survey of such derivatives by Chesnut and Wright[35] are entirely consistent with this notion.

The similarities of the shielding surfaces in somewhat larger molecules can be discovered by examining traces on the surfaces along particular displacement coordinates. It has been found[41] that the traces which display the shielding dependence on bond angle are very similar to the previous findings in the H_2O, NH_3, and PH_3 molecules shown in Fig. 2.

Of particular interest in the dependence of the shielding of the dihedral angle, which is less global in nature. It has been found that in nearly all of the systems studied, eclipsed conformations lead to greater shielding of the nuclei in the α- and β-positions, while in the staggered conformers they are most deshielded. In the small model compounds that have been studied,[50] it is also found that substitutions at the α-position influence the dihedral angle dependence of the shielding of the nucleus in the β-position, while the α-position shows insensitivity. However, this observation is true only if substitutions were restricted to the α-position. In the case of the valine model fragment, both C^{α} and C^{β} show dihedral angle dependencies that are significantly different from the smaller compounds.

3. DYNAMIC AVERAGES ON SHIELDING SURFACES, COMPARISONS WITH EXPERIMENTS

Many calculations of nuclear shielding are done at the energy-optimized molecular geometry, and the values of tensor components are compared directly with experimental chemical shift components. This has proven to be an excellent application of the *ab initio* calculations; calculations are sometimes indispensable for establishing the assignment of the tensor components.[93–97] In many cases there simply is no other information available to provide the orientations of the principal axes of the shielding tensor, which in turn provide a reliable index of the chemical bond. The chemical shift tensor is singular among the molecular electronic properties in the precision and detail with which the tensor information has been

obtained.[98] However, there are many applications in which the value of the shielding at a single point on the shielding surface does not properly account for the observations. Indeed, in every case an accurate comparison with experiment can only be done when dynamic averaging is carried out over those portions of the shielding surface which correspond to the portions of configuration space of the molecule(s) that are sampled by the motions that occur within the NMR time frame. For the intramolecular shielding surfaces this means rovibrational averaging, which requires the simultaneous knowledge of the shielding surface and the intramolecular potential energy surface. As we shall see, it is generally not sufficient to assume harmonic vibrations for this purpose. In a sense, the nuclear shielding probes the intramolecular potential surface in those regions close to the deep pockets that correspond to the immediate vicinity of the equilibrium nuclear configuration. A general treatment of the rovibrational averaging of molecular electronic properties, including the nuclear shielding provides the theoretical formalism and the perspective.[99,100] For intermolecular shielding surfaces the dynamic averaging is even more important, since the portions of configuration space that are sampled experimentally are much more extensive. In these cases it is simply not possible to consider the observed chemical shifts in terms of only one or more energetically favoured configurations.[101,102]

3.1. The temperature dependence of the shielding in a molecule

We discuss here those experimental observations that are due entirely to the dynamic averaging over the shielding surfaces. The intermolecular effects in the gas phase are easily understood to be temperature dependent since the number and nature of the collisions between molecules are clearly temperature dependent; these will be discussed in a later section. What we consider here is the observed temperature dependence of the chemical shift in the limit of zero density, where the number of collisions in sufficiently low that intermolecular interactions cannot account for the temperature dependence of the chemical shifts.[103] It was found that the shielding of ^{19}F nuclei in molecules such as CF_4, SiF_4, BF_3, SF_6,[103] and F_2[104] decreased with increasing temperature, as shown in Fig. 13. Many other examples were reported thereafter, involving not only ^{19}F but also ^{11}B, ^{15}N, ^{13}C, ^{31}P, ^{77}Se and ^{125}Te.[32–33, 106–111] These observations were postulated to arise from the existence of a shielding surface which was characterized by an expansion of the shielding in terms of nuclear displacement coordinates such as the internal coordinates or normal coordinates of the molecule.[36,112] The experimental value of the chemical shift was postulated to be the resulting thermal average of the shielding resulting from employing the thermal averages of the nuclear displacement coordinates. An equivalent approach,

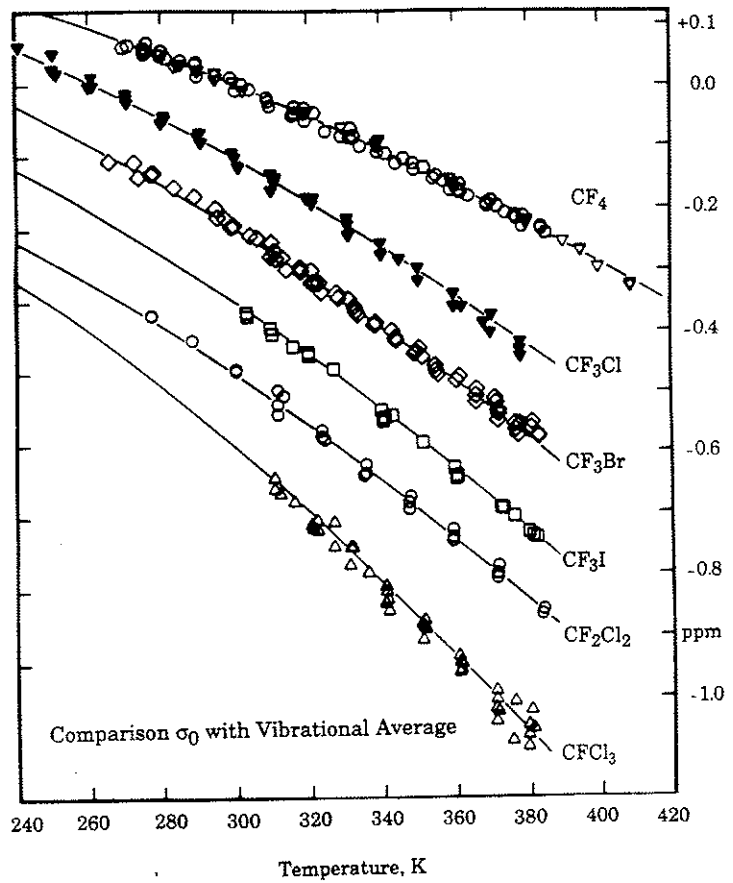

Fig. 13. The temperature dependence of the ^{19}F shielding in several fluoromethanes in the isolated-molecule limit. Reproduced from Ref. 105, with permission. The shielding scale on the y axis is set to zero for the CF_4 molecule at 300 K; the zeroes for the other molecules have been arbitrarily displaced for clarity. The curves are the one-parameter fit interpretation of the thermal average shielding obtained using a modified Urey–Bradley force field in the vibrational averaging.[105] The curvature in each case is a natural consequence of the non-linear dependence on temperature of the dynamically averaged displacements of the C–F distance from its equilibrium value in an anharmonic system.

especially for larger excursions such as inversion, is to carry out explicitly the averaging over the vibrational wavefunctions and then to average over these according to the populations:

$$\langle\sigma\rangle^{T} = \frac{\sum_{vJK} (2J+1) g_{Ns} \langle\sigma\rangle_{vJK} \exp(-E_{vJK}/kT)}{\sum_{vJK} (2J+1)\, g_{Ns} \exp(-E_{vJK}/kT)} \tag{9}$$

The rovibrational averages $\langle\sigma\rangle_{vJK}$ can be evaluated directly by integrating over the vibrational wavefunctions or in terms of the derivatives of the shielding surface with respect to nuclear displacements, as with any other molecular electronic property surface. The general formulas have been derived in terms of these derivatives and the derivatives of the potential energy surface (quadratic and higher force constants).[99,113] It was recognized fairly early that the anharmonic contributions to the mean bond displacement Δr (the so-called "mechanical anharmonicity" together with the centrifugal stretching associated with the rotational averaging for a non-rigid rotor) constitute the most important contributions.[36,112,114] There are, of course, contributions from the mean square displacement $(\Delta r)^2$ in the diatomic molecule, but these result from the counterpart of "electrical anharmonicity" in the dipole moment, that is, the second and higher derivatives of the shielding surface with respect to the bond stretch. We now know from the survey of such derivatives by Chesnut and Wright that these terms are not necessarily small.[35] The observed temperature dependencies of the chemical shifts in "isolated molecules" were reasonably large; the temperature coefficients were of the order of -0.001 to -0.034 ppm deg^{-1} for ^{19}F, for example. Here too, a nucleus such as ^{19}F with a large chemical shift range provides a large, easily measurable temperature coefficient which parallels the paramagnetic shielding of ^{19}F in the molecule, as shown in Fig. 14.[38,115] Other nuclei such as ^{13}C have considerably smaller shifts with temperature.[116] For the small molecules H_2O, CH_4, NH_3, and PH_3 whose shielding surfaces have been extensively characterized, a more complete dynamic averaging has been possible.[30,32,33,117] For the NH_3 molecule the trace on the shielding surface corresponding to variations in the inversion coordinate has been used to carry out the full dynamic averaging using the numerical vibrational wavefunctions obtained by solving the nuclear motion problem using the empirical potential energy surface.[32] For these four molecules, the full dynamic averaging has been possible since both the anharmonic potential surface and the shielding surface are known. The complete set of symmetry coordinates of the molecule has been used to calculate all the contributions to the shielding, including higher-order terms. When the dynamic averaging is carried out for more than one isotopomer of the molecule, then the mass dependence of the dynamically averaged

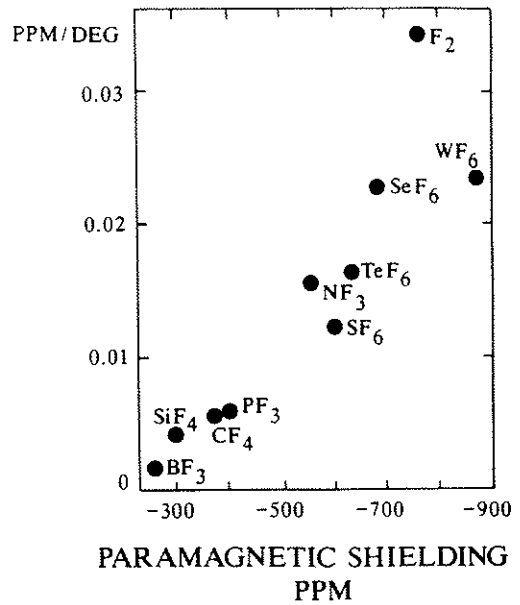

Fig. 14. The temperature coefficient of the shielding of ^{19}F in the binary fluorides in the isolated-molecule limit correlate with the paramagnetic shielding in these molecules (obtained from the absolute shielding and the calculated diamagnetic shielding using Flygare's method). Reproduced from Ref. 115, with permission.

shielding can also be obtained. The temperature dependence of the shielding of the ^{13}C in CH_4, the ^{15}N in NH_3, and the ^{31}P in PH_3 relatively small and that of the ^{17}O in H_2O has not been measured yet. Nevertheless, these comprehensive studies provide the basis for the interpretation of the observed large temperature dependences in other molecules and the first accurate calculations of the isotope effects on the chemical shifts in polyatomic molecules. The magnitudes of the rovibrational corrections in some small molecules shown in Table 1 illustrate that these are not small corrections and should always be taken into consideration in making a comparison between the calculated shielding at the equilibrium molecular geometry and the experimental absolute shielding.

Averaging over the torsional motions could be important, especially in the case of saturated carbon nuclear sites which have intrinsically small derivatives with respect to bond extension. It has been suggested that the averaging over torsional motions provides increased shielding with increasing temperature.[46,120] Bennett and Raynes have found that the temperature coefficients of ^{13}C in molecules having CH_3 groups that can undergo torsional motion about a carbon–carbon single bond are positive.[116,121] The temperature coefficients of the shielding in conformationally inhomogeneous

Table 1. Typical vibrational corrections $[\sigma(300\,K)-\sigma_e]$, ppm.

Term[a]	CH_4[117]	NH_3[32]	PH_3[33]	H_2O[118]	H_2Se[c]
P_r	−4.368	−7.69	−9.16	−10.835	−43.3
P_{rr}	−1.696	−3.59	−5.97	−4.824	−19.3
$P_\alpha + P_{\alpha\alpha}$	+2.573	+2.49	+2.25	+1.524	+3.7
Other	−0.10	−0.02	+0.10	+0.565	Neglected
Total	−3.591	−8.81	−12.78	−13.57	−58.9

[a] P_r denotes terms involving the first derivative of nuclear shielding with respect to the bond stretch P_{rr} denotes terms involving the second derivative $P_\alpha + P_{\alpha\alpha}$ include terms in the first and second derivatives of shielding with respect to bond angle deformation.
[b] Mixed terms and higher order terms.
[c] Calculated by Ref. 119 based on the points on the *ab initio* shielding surface of Ref. 34.

n-butane and iso-pentane are of the same order of magnitude as for the conformationally homogeneous ethane, propane, isobutane, and neopentane molecules. Thus, Raynes and Bennett make the important point that any attempt to obtain shielding values for individual conformers from the measurement of the temperature dependences of carbon shielding based on the notion of temperature-dependent equilibria between a small number of conformers is naive, since this notion ignores the contributions of geometries of the torsionally distorted conformers.[121]

3.2. Isotope effects

The mass dependence of the chemical shift was discovered even earlier than the temperature dependence;[122] however, it was not until the recognition of the shielding surface that a single theoretical formalism could be established to explain both phenomena.[36,37] It is in the context of the Born–Oppenheimer separation that the possibility of considering a molecular electronic property surface, such as the shielding surface, is achieved. In this context the shielding surface, being entirely an electronic property calculated for the various configurations of the nuclei, is the same for all isotopomers of the molecule. The observed mass-dependence of the shielding is then entirely a result of the differential dynamic averaging in a heavy isotopomer compared to the light one. When the observed nucleus itself is isotopically replaced, the shielding average is changed. This is the primary isotope effect and is most conveniently observed indirectly as the chemical shift between two different molecular species. The secondary isotope shift is observed when the mass of an atom one or more bonds away is different. Although the shielding difference is best written out in terms of the two isotopomers, such as $[\sigma(^{15}N,\ ^{15}NH_3) - \sigma(^{15}N,\ ^{15}ND_3)]$, the commonly observed additivity in the isotope effects on shielding[122–124] allows the isotope shifts to be reported in terms of single substitutions, as follows: ${}^n\Delta^{13}C(^{2/1}H)$ is the shielding difference between the normal and the deuterated isotopomer for a single substitution n bonds away from the observed ^{13}C nucleus.[125] The isotope shift is ubiquitous and literally thousands of examples are found in the literature.[122,126] The isotope shifts come about because the dynamic averaging by the heavy isotopomer involves smaller amplitudes of nuclear motion than the dynamic averaging by the light isotopomer over the identical shielding surface.[37] On the average, the lighter isotopomer samples a larger region of the shielding surface than does the heavier isotopomer in its excursions away from the equilibrium molecular geometry. We have seen the global shape of the shielding surface in Fig. 1. When the point of minimum energy (equilibrium geometry) happens to fall in that part of the shielding surface in which the shielding is sharply decreasing with bond extension, then the larger amplitudes of motion in the averaging of the lighter molecule over the regions of the shielding surface that correspond to the immediate vicinity of the equilibrium arrangement produces greater deshielding than does the smaller amplitudes of motion of the heavier molecule. This leads to the usually observed negative sign of the isotope shift. On the other hand, in those cases where the minimum on the potential energy surface happens to fall on the other side of the shielding surface where bond stretching leads to increased shielding, as for the Li nucleus, the sign of the isotope shift is opposite to the usual; the larger excursions of the light molecule leads to a more shielded average than for the heavy molecule. Indeed, for isotopic substitution one to three bonds away, Li isotope shifts in organolithium compounds are found to be opposite to the usual sign.[127,128] Now consider the trace of the shielding surface along the bond angle deformation. This portion of the shielding function having a minimum at the tetrahedral angle, the averaging over the bond angle deformations generally leads to increased shielding when the equilibrium bond angle is not too far from tetrahedral.[30,32] However, it has been found that the isotope shift is dominated by the bond stretching,[33] even in the case of NH_3 where averaging over the inversion coordinate is complete; see for example the relative contributions in Table 2. It is not too surprising, then, to find that one-bond isotope shifts are fairly predictable in sign.[40] The trends in isotope shifts have been explained theoretically,[40,56] including the additivity,[134] the dependence on the fractional change in mass,[135] and the observed linear dependence on $[1-(\mu/\mu')^{1/2})]$ or the (m′-m)/m′ factor for a series of isotopes of the same element.[115,135] The isotope shifts in isolated molecules can now be said to be completely understood and can be calculated, in principle. For example, for the CO molecule, the observed temperature dependence of the ^{13}C shielding, the ^{13}C isotope shifts due to $^{17}O/^{16}O$ and $^{18}O/^{16}O$ substitution, and the ^{17}O shift due to $^{13}C/^{12}C$ substitution, all have been calculated[136] and found to agree fairly well with experimental

Table 2. Isotope shifts $[\sigma^X(XH_n) - \sigma^X(XD_n)]$, ppm, calculated for ^{13}C, ^{15}N, ^{31}P, ^{17}O and ^{77}Se nuclei.

Term[a]	CH_4[129]	NH_3[32]	PH_3[33]	H_2O[118]	H_2Se[b]
P_r	−1.169	−2.05	−2.44	−2.847	−11.66
P_{rr}	−0.453	−0.97	−1.68	−1.316	−5.59
$P_\alpha + P_{\alpha\alpha}$	+0.686	+0.66	+0.67	+0.404	+1.25
Other[c]	−0.042	−0.004	0.002	+0.08	Neglect
Total	−0.978	−2.36	−3.45	−3.68	−16.0
Expt	−0.774[130]	−1.87[124]	−2.53[131]	−3.09[124d]	−14.04[132]

[a]Same definitions as in Table 1.
[b]Calculated by Ref. 119 based on the points on the *ab initio* shielding surface of Ref. 34.
[c]Mixed terms and higher-order terms.
[d]In the gas phase a value of −4.04 ppm has been reported.[133]

values.[106,137] The isotope shifts of ^{17}O in H_2O and D_2O, ^{13}C in $^{13}CH_nD_{4-n}$, ^{15}N in $^{15}NH_3$ and $^{15}ND_3$ and ^{31}P in PH_3 and PD_3 have all been calculated using the full shielding surfaces for these nuclei.[30,32,33,117] A complete calculation for larger molecules may be limited by the lack of accurate potential energy surfaces or simply by the large number of nuclear displacement coordinates. Therefore, the knowledge gained from complete calculations using all the symmetry coordinates in these small molecules helps to gauge the limits of applicability of using a less complete picture, such as, for example, using a dynamic average of a local displacement coordinate at the substitution site coupled with the shielding derivative with respect to that remote displacement, as we shall see below.

The magnitude of the isotope shift depends on several factors which have been discussed in detail in previous reviews.[40,56] (a) The magnitude of the isotope shift is a function of the observed nucleus and reflects its chemical shift range. The sensitivity of the nuclear shielding (the derivatives of the shielding surface at the equilibrium geometry are large) of ^{129}Xe leads to isotope shifts as large as −0.58, −0.52, and −0.69 ppm for $^{18}O/^{16}O$ substitution in $XeOF_4$, XeO_2F_2, and $XeOF_3^+$.[138] The shielding sensitivity depends on $<a_0^3/r^3>$ for the atom, and the shielding derivatives appear to scale accordingly. The shielding surfaces of related diatomic molecules in the vicinity of the equilibrium geometry (e.g. the surfaces of ^{35}Cl in ClF and ^{19}F in F_2, ^{35}Cl in HCl and ^{19}F in HF, ^{23}Na in NaH and ^6Li in LiH) have been found to be superimposable with each other upon using a scaling factor $R_e<a_0 3/r^3>$.[23] (b) Upon substitution with a heavier isotope the NMR signal of the nearby nucleus usually shifts towards lower frequencies (higher shielding). The survey of *ab initio* derivatives of shielding surfaces by Chesnut and Wright[35] confirms the preponderance of negative first (and second) derivatives. (c) The magnitude of the shift is related to the fractional change in mass upon isotopic substitution. This is directly a result of the dynamic averaging and has been verified by calculations of vibrational

averages.[115] The mass factor comes from the mean bond displacement and mean square amplitudes, that is, the amplitudes of motions on the surface depend in an explicit way on the masses of the atoms undergoing the excursions, and are best treated in terms of curvilinear internal coordinates, taking into account the symmetry of the whole molecule. Nevertheless, some simplifying assumptions lead to the proportionality of the isotope shifts of multiple isotopes on the mass factors $[1-(\mu/\mu')^{1/2}]$ or (m'-m)/m' that had been derived for diatomic molecules[37,135] and found empirically valid for polyatomics.[115] (d) The additivity exhibited by isotope shifts is also a consequence of the dynamic averaging and has been theoretically derived[134] and experimentally verified exhaustively. Where sizeable deviations from additivity occur, intermolecular effects have been found to play an important role.

There are some qualitative trends which have been observed, correlating isotope shifts with molecular structure, which are less universal in nature but nevertheless useful on occasion. These trends were attributed entirely to the dependence of the derivatives of the shielding surfaces on various indices of the chemical bond.[39] *Ab initio* calculations of such derivatives reaffirm these notions which had been based entirely on experimental data and the dynamic averaging model:

(1) One-bond isotope shifts tend to increase with increasing bond order (and the accompanying decreasing bond length) between the observed nucleus and the substituted atom. The nature of the chemical bond determines the shape of the shielding surface at the equilibrium geometry; thus, Chesnut's survey of shielding derivatives shows trends with respect to bond orders[35] (as in Fig. 3).

(2) When an end atom is observed, the isotope shift correlates with the chemical shift of the observed nucleus; that is, the less shielded nuclei have larger isotope shifts. This is a parallel behaviour to that of the temperature coefficient shown in Fig. 14. Both correlations had been interpreted to mean that the first derivatives of shielding surfaces with respect to bond extension correlate with the shielding value at the equilibrium geometry.[38] ^{19}F and ^{17}O shielding surfaces have subsequently been found to possess derivatives that do correlate with the shielding values at equilibrium. Thus, ^{13}C in C=O functional groups and ^{19}F in fluorocarbons give a nice experimental correlation in isotope shifts (or temperature coefficients) vs. shielding and also a nice correlation between *ab initio* shielding derivatives and shielding. When observing other than terminal atoms, the situation becomes clouded by the multiple terms that contribute to the shielding in various bonding situations, thus, derivatives with respect to stretching of one of the bonds do not correlate well with shielding in these situations.

(3) The isotope shifts tend to be larger in the presence of a lone pair or a net negative charge, or when electronegative substituents are introduced at the nuclear site, as in H_2O, H_3O^+, NH_3, NH_4^+, PH_2^-, PH_3, PH_4^+, SnH_3^-, SnH_4, SnH_3^+.[124,131,139,140] Where they had been calculated, the shielding derivatives are indeed found to be larger negative in H_2O than in H_3O^+, NH_3 than in NH_4^+, PH_3 than in PH_4^+, for example. Table 2 shows that in those cases where the multidimensional shielding surface has been calculated in the immediate vicinity of the equilibrium geometry and the complete dynamic averaging has been done properly, the largest contributions to the isotope shifts are due to the terms in Δr and $(\Delta r)^2$. With estimates for the thermal averages of Δr and $(\Delta r)^2$ being readily available,[135] isotope shifts can be used to estimate shielding derivatives directly from the experimental data.[40,56]

The isotope shift depends in principle on all the shielding derivatives and the dynamic averages of all the internal coordinates of a molecule.[37] Isotope shifts due to substitution at a remote bond would at first glance involve only higher-order terms since the local mass effect on the dynamic averaging occurs primarily at the substitution site which is remote from the nucleus whose shielding is observed. On the other hand the mass effects at the bonds directly attached to this nucleus are expected to come entirely from the coupling between vibrations involving displacements of the atoms where isotopic substitution takes place and those involving displacements of the bonds directed to the observed nucleus. Of these two types of higher-order terms, it was predicted that the secondary shielding derivative with respect to remote bond extension together with the primary mass effect at the substitution site dominates the isotope shifts over two or more bonds.[55] This means that these long-range isotope shifts contain electronic information and can serve as a gauge of the electronic transmission through bonds between the observed nucleus and the substitution site, certainly more useful than a gauge of long-range coupling of local vibrational modes. The 2-bond and 3-bond isotope shifts had been attributed to the secondary derivative, that is the non-negligible derivative of the shielding with respect to the stretching of the remote bond at which the isotopic substitution has taken place.[55,141,142] Chesnut's survey of shielding derivatives indeed shows the importance of secondary derivatives.[35] The usual fall-off of the magnitude of the isotope shift with the remoteness of the substitution had been explained in terms of the secondary derivatives being generally smaller than the primary derivatives.[40] Chesnut and Wright find that this is not always true; there are some secondary derivatives that are comparable to and occasionally even larger than the primary derivatives.[35] Also, these derivatives can be of either sign, although large values are usually negative. The observed correlations of 2-bond and 3-bond isotope shifts with the

corresponding coupling constants[122,143] indicate involvement of the electronic transmission path between the nuclear site and isotope substitution site, which further supports the importance of the secondary derivatives. The fall-off with distance from the resonant ^{13}C nucleus in an aromatic system is not nearly as fast as in saturated ones. For example, in adamantane and derivatives, the isotope shifts for $n = 1$–5 bonds away are 400–800 ppb, 85–200 ppb, 8–46 ppb, 0–20 ppb, and 0–10 ppb,[144] whereas for $n = 1$–3 bonds in aromatic systems they are 190–380 ppb, 50–213 ppb, 28–100 ppb.[145]

The remote secondary shielding derivatives associated with long-range isotope shifts can be of either sign, and even in the same molecule both signs can be obtained. To illustrate this, we consider norbornene, in which the deuterium-induced ^{13}C shifts have all been measured and found to be of both signs, negative (usual) for carbons 1–4 and positive (unusual) for carbons 5, 6, and 7 upon deuteration at the ethylenic carbon.[146] We have

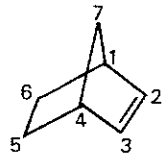

carried out *ab initio* GIAO calculations of the traces corresponding to the variation of the symmetry coordinate, the symmetric stretch, $S_1 = [\Delta r(C_2–H_2) + \Delta r(C_3–H_3)]$ in the ^{13}C shielding surfaces of all carbons in this molecule.[147] These calculations reveal that in the vicinity of the equilibrium geometry, the traces for $^{13}C_1$ and $^{13}C_4$, $^{13}C_2$ and $^{13}C_3$ shielding decrease monotonically with increasing S_1, whereas the $^{13}C_5$, $^{13}C_6$ and $^{13}C_7$ shielding definitely increase (albeit only slightly) with increasing S_1. Thus, in the same molecule the ^{13}C shielding derivatives with respect to remote C–H stretching are of opposite signs, consistent with the corresponding signs of the observed isotope shifts.

3.3. Intermolecular shifts

Solvent shifts can sometimes involve the formation of hydrogen bonds or the formation of an association complex. For example, the very useful shifts that distinguish between the left- and right-handed forms of a molecule by the different chemical shifts they exhibit in association with a chiral solvent are entirely due to differential intermolecular shieldings, the averages over the configurations of the diastereomer R–C being slightly different from the averages over the configurations of the diastereomer S–C when solvent C is chiral. Observed chiral shifts are of the order of 0.025 ppm for ^1H,[148] 0.036 ppm for ^{19}F,[149] and 0.164–0.685 for ^{15}N.[150] In these applications, the

observed nucleus generally has to be fairly close to the chiral centre, but not necessarily. A dramatic example is a chiral auxiliary reagent with a ^{77}Se nucleus in a selenocarbonyl group which exhibits sufficient sensitivity to report on more distant chiral centres. The diastereomers which result from the coupling of the reagent to (R,S) lipoic acid have the chiral centre of the lipoyl group eight bonds away from the ^{77}Se, yet the ^{77}Se NMR spectrum features two clearly resolved resonances separated by 0.119 ppm.[151] Because stereospecific interactions between such solute and solvent molecules at short range lead to a correlated intermolecular geometry, corresponding nuclei in S and R enantiomers in the diastereomeric pairs will experience different shieldings via the usual mechanisms operating in intermolecular effects on shielding, leading in many instances to an experimentally significant shielding non-equivalence. The differential averages over the orientations of the benzene solvent molecules for a rod-shaped solute and a spherical solute molecule account for the observed chemical shifts in aromatic solvents, which was explained by Buckingham *et al.* in terms of the anisotropy of the magnetic susceptibility of the aromatic solvent molecules.[152] What we discuss in this section, however, are those theoretically calculable intermolecular shifts, which serve as quantitative paradigms for the dynamic averaging over the intermolecular shielding surfaces where no specific interactions or associations need be invoked, and can therefore serve as the examples of ever-present intermolecular shieldings.

3.3.1. The chemical shift in the gas phase

The shielding, just as any other molecular electronic property measured in the bulk, can be expressed in terms of an expansion in the density:[153]

$$\sigma(T,\rho) = \sigma_0(T) + \sigma_1(T)\rho + \sigma_2(T)\rho^2 + \sigma_3(T)\rho^3 + \qquad (10)$$

where $\sigma_1(T)$ is the second virial coefficient of nuclear shielding. The early measurements of the virial coefficients of shielding involved protons in molecules such as HCl. The interpretation of these shifts by Raynes, Buckingham and Bernstein was largely tied up with the notion that the intermolecular shifts could be viewed in terms of electric field effects.[89] With the use of the Drude model this was extended to fluctuating electric fields to represent the dispersion contributions,[89] not so important in protons.[154] However, the large magnitudes of the intermolecular shifts of ^{129}Xe in mixtures of Xe with rare gases and other molecules severely tested the model, requiring a rather large dispersion contribution to account for the large second virial coefficients of shielding for this nucleus.[155] Furthermore, the rather large temperature dependence also presented a problem.[156] The lack of reliable intermolecular potentials at that time left the problem unresolved. Reliable calculations of the B coefficient, supposedly the same

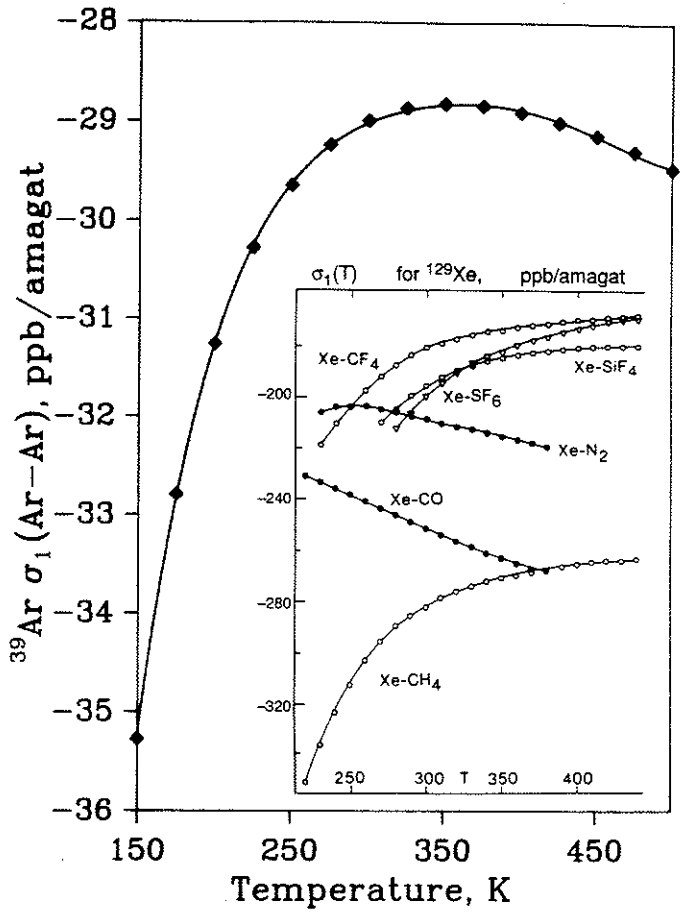

Fig. 15. The second virial coefficient of shielding $\sigma_1(T)$ for ^{39}Ar in argon gas,[24] calculated from the '*ab initio* shielding surface and the potential surface from Aziz–Chen.[29] Most experimental $\sigma_1(T)$ curves exhibit the behaviour similar to that calculated for argon below 350 K, that is, the magnitude of the density coefficient of the chemical shift in the gas phase decreases with increasing temperature. There are, however, at least two examples (Xe–CO and Xe–N_2) of behaviour like the calculated curve above 350 K.

one for the fluctuating electric fields as for a uniform static field, were not available until a much later date. Given the theoretical shielding surfaces for rare gas pairs,[23,24] and the reliable potential surfaces now available, it is possible to carry out the proper averaging to obtain the second virial coefficients as a function of temperature. An example is shown for the ^{39}Ar in Ar_2 virial coefficient of shielding in Fig. 15. The behaviour of this $\sigma_1(T)$

over a wide temperature range is typical of most of the experimental ^{129}Xe $\sigma_1(T)$ values that are known. The sign is negative at all temperatures, that is, intermolecular effects are generally deshielding.[101,114] The temperature dependence that has been observed for most of the ^{129}Xe $\sigma_1(T)$ is such as to make the deshielding effect more exaggerated at lower temperatures. However, there have been at least two examples, Xe in CO and Xe in N_2 mixtures, in which the behaviour is opposite.[157] We see in Fig. 15 that both behaviours are present; it is only the range of temperatures relative to the well depth that limits the observations to one or the other side of the maximum in the $\sigma_1(T)$ function in most cases. The calculated $\sigma_1(T)$ for the ^{129}Xe nucleus in Xe–Ar, Xe–Kr, and Xe–Xe interactions in the gas phase are shown in Fig. 16. The agreement with the experimental data is reasonably good: the signs are correct, the relative magnitudes are correct, and the temperature dependences are about right. With this, the density dependence of the chemical shift in the gas phase may be said to be understood. The intermolecular shifts of molecules with structure are rather more difficult to calculate because not only the distance but the orientations have to be considered in constructing the shielding surface and in the dynamic averaging. There are some ^{13}C σ_1 data which have recently been measured; these are also found to be uniformly negative.[116] Other nuclei for which fairly large $\sigma_1(T)$ values have been measured in the gas phase are ^{19}F nuclei in various fluorocarbons, with values ranging from -0.0048 to -0.045 ppm amagat^{-1}.[101]

The striking examples of intermolecular shifts that have positive σ_1 are the shifts of N nuclei in the types of nitrogen environments that involve low-lying n-π^* excited states in the shielding, for example, HCN, MeCN, pyridine.[159] To interpret these observations it is necessary to calculate the whole shielding surface for at least the dimer and then do a proper averaging over the surface. This has not yet been done; however, there is at least one configuration for the dimer in which increased N shielding compared to the monomer MeCN has been calculated.[160] HCN is known to form linear hydrogen-bonded complexes $(HCN)_n$ which leave the C–H bond intact upon exchange. A proper average would allow the size of the n-mers to vary. This, alas, is not yet possible. In the following section, however, we consider a system in which a proper average over all the configurations of the n-mer is carried out at each temperature and the average chemical shifts agree with experiment.

3.3.2. The average chemical shifts of Xe in zeolites

Physisorption is a result of intermolecular interactions between an adsorbate and the atoms of the host matrix. The sorbate–sorbate interactions affect the observed adsorption isotherms and other properties including diffusion of the sorbate molecules through the host lattice. One particularly interesting

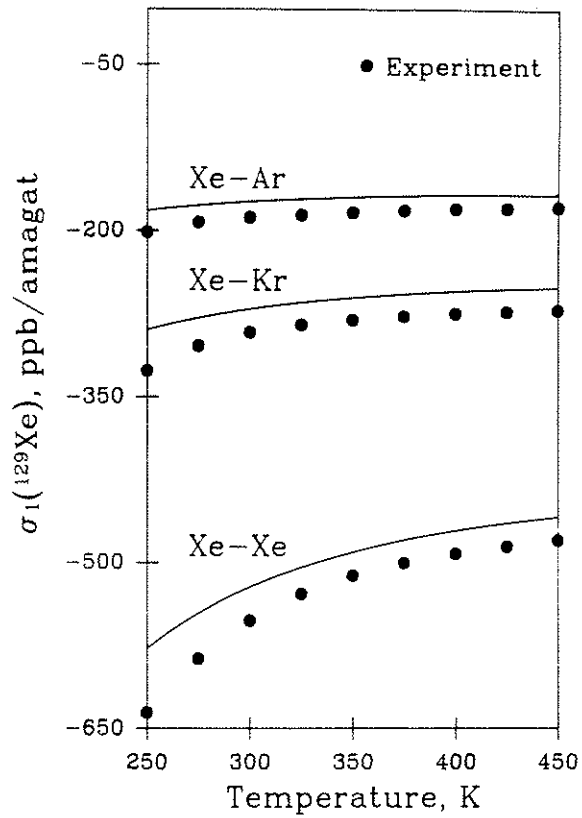

Fig. 16. The second virial coefficients of shielding $\sigma_1(T)$ for ^{129}Xe for Xe in Ar, Xe in Kr, and Xe in pure Xe gas have been calculated from the *ab initio* Ar–Ar shielding surface scaled to ^{129}Xe in Xe–Ar, Xe–Kr and Xe–Xe respectively. The results agree with experiment in sign, in relative magnitudes, and in the temperature dependences. Experimental values are from Refs 156 and 158.

example of this phenomenon is the intermolecular shifts of the Xe nucleus due to the interactions with the atoms of a zeolite. The ^{129}Xe chemical shift in the limit of extremely low loading of xenon in the zeolite (relative to the isolated Xe atom) has been found to vary greatly depending on the internal structure of the zeolite and the types of counterions that are present in it. Furthermore, the effects of the sorbate–sorbate interactions on the chemical shifts are very large, with the ^{129}Xe chemical shift increasing with increasing average number of Xe atoms per unit cell. These shifts are of the order of tens and hundreds of ppm. Since the Xe–Xe shielding surface has been derived, it should be possible to calculate the grand canonical average of the ^{129}Xe chemical shift under those conditions in which the major contributions

to the shielding are indeed due to the sampling of all possible Xe–Xe distances. In order to do this, we need to consider a shielding surface that can be calculated on the fly, changing with the numbers of neighbours as the numbers of sorbate atoms fluctuate in the grand canonical ensemble. We have seen already in the example of the triangular and linear Ar_3 clusters that as long as the Ar atoms do not get much closer than about $0.9r_0$, the isotropic shielding contributions can be obtained by additivity. We therefore construct the ^{129}Xe shielding surface as we go, summing up over all the atoms that are sufficiently close (less than 12 Å). An approximate shielding surface has been constructed to include interactions with the oxygen atoms in the zeolite framework and the Na^+ ions which provide the counterbalancing charges in this particular aluminosilicate (zeolite NaA). The observations in this particular zeolite are even more detailed than in all other cases. Here, what is observed is not an average chemical shift under fast exchange of the Xe with a very large number of cavities containing a varying number of Xe atoms, but rather the individual chemical shifts of trapped clusters of Xe atoms, Xe_1, Xe_2, Xe_3, . . . up to Xe_8. The chemical shifts have been measured as a function of temperature and these pose dynamical averaging challenge for the theory.[64] Typical spectra of samples of xenon in zeolite NaA are shown in Fig. 17. The shielding of the ^{129}Xe in the Xe_n clusters changes according to n; the most deshielded nuclei are in the Xe_8 cluster. It is of interest that the cluster shift is in the direction given by $\sigma_1(T)$ observed in the gas phase. However, the incremental change is not a fixed amount but increases slightly in going from 1 to 6. Furthermore, there is a big change in shielding in going from Xe_6 to Xe_7 and then again in going from Xe_7 to Xe_8. These are all consequences of the dynamic averaging over these various shielding surfaces. Given the potential function for the interaction of a single Xe atom with the lattice and the Na^+ ions, given that the total potential energy is assumed to be a sum over all the pairwise interactions at distances less than some cutoff distance, and given the interaction potential function for the Xe–Xe interactions, likewise taken to be pairwise additive, then the properly weighted large number of configurations (a million or so) can be summed in a Grand Canonical Monte Carlo (GCMC) scheme. At each of these configurations the shielding of every Xe nucleus is calculated. Thus, the average chemical shift of a ^{129}Xe nucleus can be calculated. The isotropic shielding averaged over all the Xe atoms in the cluster is separately stored for each of the eight cluster types so that the average chemical shift for each Xe_n can be obtained. This is done at each temperature. The temperature and the chemical potential of the adsorbed xenon are set, while the numbers of xenon atoms are allowed to fluctuate. The averages at various temperatures can then be compared with the experimental chemical shifts at these temperatures. We show the results in Table 3 and in Fig. 18. The agreement of the GCMC average with experiment is excellent, especially considering that there are no adjustable parameters here; none of

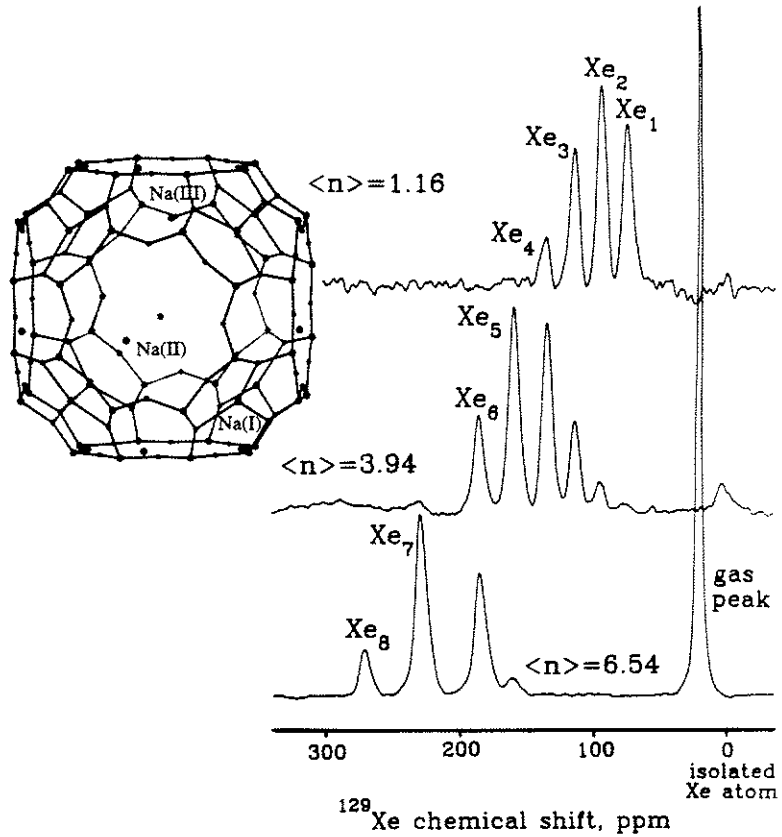

Fig. 17. The ^{129}Xe NMR spectra of xenon atoms trapped in the alpha cages of zeolite NaA, showing the large intermolecular chemical shifts which are absolutely referenced to an isolated Xe atom. The observed $^{129}Xe_n$ chemical shift is a thermal average over all sampled configurations of the Xe_n in an alpha cage. The intensities of the signals from the cages containing 1, 2, 3, . . ., 8 Xe atoms provide the distributions of occupancies in each of the three samples at low, medium, and high xenon loading.[64,102]

the experimental values has been used to adjust any of the chemical shifts. The calculated and experimental quantities being compared are in absolute terms, that is, the shieldings are relative to the free Xe atom in both calculation and experiment. A very important point to be made here is that the proper averaging had to be carried out. There is a large number of local minima in the configuration space of each of the clusters. The shielding of Xe in these minimum energy configurations for the clusters have also been calculated. It is important to note that the shieldings from these minimum

Table 3. Shielding of Xe_nclusters trapped in the alpha cages of zeolite NaA, ppm.

n	$<\sigma(Xe_n) - \sigma(\text{free atom})>$		Increments $<\sigma(Xe_n)> - <\sigma(Xe_{n+1})>$	
	EXPT[64]	GCMC[102]	EXPT[64]	GCMC[102]
1	-74.8	-77.2		
2	-92.3	-92.6	17.5	15.5
3	-111.7	-109.6	19.4	17.0
4	-133.2	-129.9	21.5	20.3
5	-158.4	-155.4	25.2	25.5
6	-183.5	-184.2	25.1	28.9
7	-228.3	-226.0	45.1	41.7
8	-272.3	-269.7	43.7	43.7

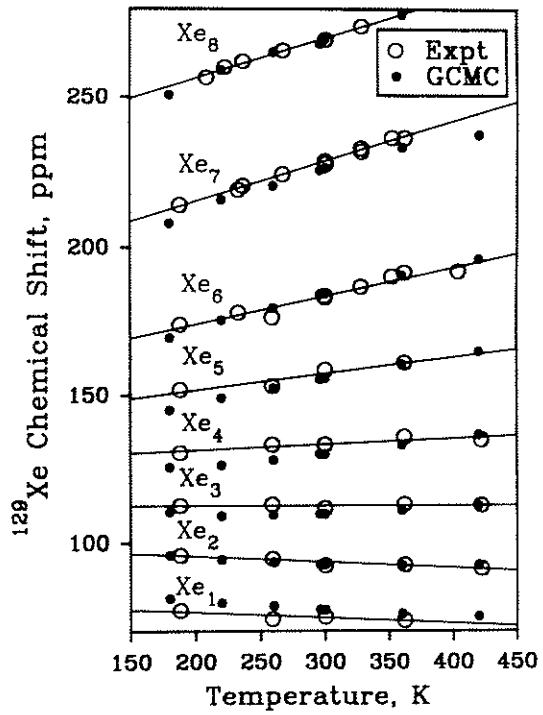

Fig. 18. The temperature dependence of the average ^{129}Xe chemical shift in each of the Xe_n clusters trapped in the alpha cages of zeolite NaA is reproduced by taking a Grand Canonical Monte Carlo average, using a ^{129}Xe shielding surface that is a sum of pairwise intermolecular shielding functions derived from *ab initio* calculations.[64,102]

energy configurations provide chemical shielding increments from one cluster to the next that are not at all like the ones obtained from the GCMC averaging. The observed incremental shifts from one cluster to another cannot be reproduced if only the minimum energy cluster structures are considered. The proper average over the configurations dictated by the multidimensional potential energy surface had to be carried out. This dynamic averaging becomes even more important when the molecule is freely migrating from one cage to another, sampling a variety of occupancies within the NMR time scale in zeolites with open cages. The single peak observed there provides a chemical shift that is averaged not only over the possible configurations of the xenon atoms within one cage, but also averaged over the distribution of occupancies throughout the zeolite.

The gas-to-adsorbate shift, that is, the chemical shift of a single Xe atom in a zeolite cavity, was also well reproduced in this case. However, this is more fortuitous than real, given that the Xe–zeolite shielding function was only approximate.

3.3.3. Gas-to-liquid and gas-to-solution shifts

In the above example, the number of atoms involved in the averaging was finite. Although the zeolite contributions to the shielding changed somewhat from cluster to cluster, the major shielding differences came from the varying magnitudes of Xe-Xe contributions to the shielding. We now consider a situation more comparable to the single average shielding observed under fast exchange conditions. An obvious intermolecular shift is the gas-to-liquid shift or the gas-to-solution shift. In Fig. 19, the ^{19}F chemical shifts in the liquid and in the vapour observed in equilibrium with it are temperature dependent due to intermolecular interactions and intramolecular vibrational averaging. On the other hand, the gas-to-liquid shift $[\sigma_{liq} - \sigma_{vap}]$ is entirely an intermolecular shift and is a function of the change in $[\rho_{liq} - \rho_{vap}]$ with temperature. Note that the gas-to-liquid shifts are expected to approach zero at the critical temperature. For each of four monosubstituted fluoroethenes, each distinct nucleus in the same molecule has an intermolecular shift that is related to its distance from the molecular centre of mass, a nuclear site effect that comes from slightly different dynamic averaging in each case. Note that for a fluoroethene with a substituent lighter than F, the order of intermolecular shifts is different than for a fluoroethene with a substituent heavier than F. It is found that the σ_1 are in the same rank order as the $[\sigma_{liq} - \sigma_{vap}]$ in Fig. 19. When the substituent is H, the σ_1 values at 300 K are -11.8, -19.0, -18.9 ppb amagat^{-1} for F_A, F_B, F_C, respectively. For fluoroethene itself, it is -17.8 ppb amagat^{-1}. When the substituent is Cl, the σ_1 values at 300 K are -26.7, -25.1, -24.8 ppb amagat^{-1} for F_A, F_B, F_C, respectively; when it is Br, the σ_1 values at 300 K are -31.4, -26.8, -26.7 ppb amagat^{-1}

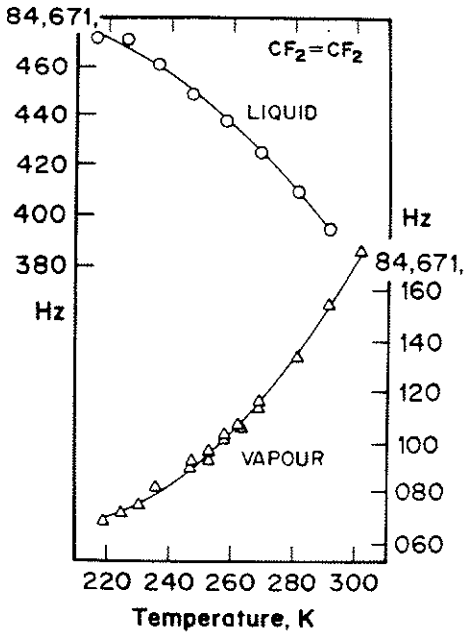

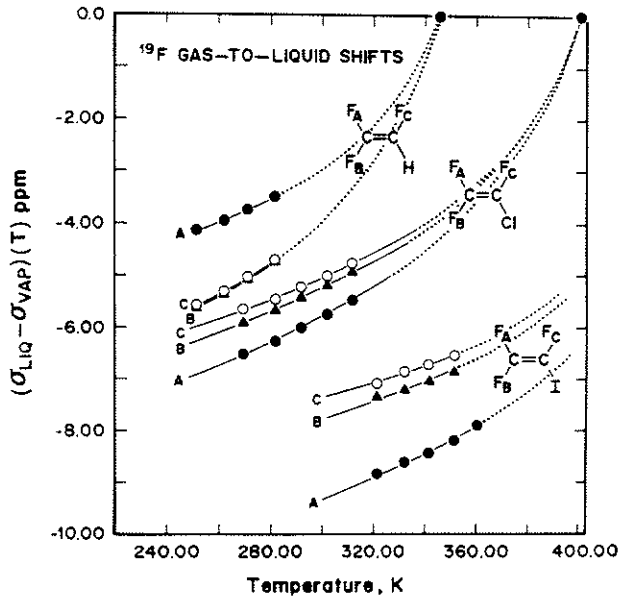

Fig. 19. The temperature dependence of the gas-to-liquid shifts in fluoroethenes. Reproduced from Ref. 161, with permission.

Table 4. Experimental gas-to-liquid shifts.

Nucleus	Molecule	ppm	T, K	Ref.
^{1}H	NH_3	–1.75	300	162
	H_2O	–4.368	298.2	163
^{17}O	H_2O	–36	300	133
^{13}C	C_6H_6	–1.5	300	164
	TMS	–4	300	164
	HCN	–7.68	346.6	159
^{15}N	NH_3	–19.5	300	162
	HCN	+10.4	346.6	159
	MeCN	+11.3	227.5	165
^{19}F	CF_3Cl	–3.65	280	166
	CF_3I	–5.305	280	166
	$CFCl_3$	–5.994	340	167
	SeF_6	–4.8	300	115
	WF_6	–7.4	300	115
	CH_3F	–7.7	260	168
	ClF	–25.6	220	169
^{31}P	P_4	–77	526	170
^{77}Se	SeF_6	–1.38	300	115
	H_2Se	–120	300	115
^{129}Xe	Xe	–200	244	171–172

respectively; and when the substituent is I, the σ_I values at 300 K are −61.8, −51.2, −49.7 ppb amagat^{-1} respectively for F_A, F_B, F_C.[161] To calculate these intermolecular shifts due to interactions between freely rotating molecules, the ensemble average has to be carried out over all orientations and distances; a nucleus that is further from the centre of mass will sample somewhat shorter interaction distances than one that is closer to the centre of mass in the same molecule. Intermolecular shielding functions of the form similar to those in Fig. 10 have larger negative values at shorter distances. Thus, the ensemble average $\sigma_1(T)$ is largest negative for the nucleus which is furthest from the centre of mass. This is indeed what is found consistently in each of the substituted fluoroethenes. Evidence such as this underscores the importance of dynamic averaging to the understanding of observed chemical shifts.

Many gas-to-liquid shifts have been measured for ^{19}F nuclei, and a selected few for other nuclei. It is interesting to compare the relative sensitivity of different nuclei to deshielding effects of the surrounding medium. Table 4 shows a few examples. The ^{17}O in H_2O and ^{77}Se in H_2Se gas-to-liquid shifts are proportionately large, as may be expected, according to either $\langle a_0^3/r^3 \rangle$ for the atoms or the ranges in the O and Se chemical shifts. The magnitudes of these shifts of course depend on temperature and the density of the liquid. Where exactly the same set of solvents is used and

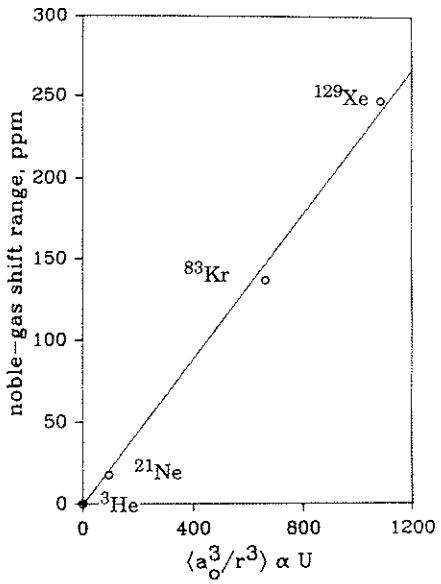

Fig. 20. The ranges of the chemical shifts of the rare gas atoms dissolved in the same set of organic solvents[173–176] are proportional to the scaling factors $<a_0^3/r^3>\alpha U$ for the atom.

the chemical shifts of the solutes (in the limit of infinite dilution) can be compared, some interesting trends emerge. For example He, Ne, Kr, and Xe solution shifts have been measured in exactly the same set of organic solvents.[173–176] It is found that the chemical shift range in these solvents correlates with some properties of the rare gas. In Fig. 20 we show the correlation with the fundamental quantities which are properties of the rare gas atom in question, the same factors that have been used for scaling the shielding surfaces: $<a_0^3/r^3>\alpha U$. The sensitivity of a nucleus to the deshielding effects of intermolecular interactions depends on the rare gas atom's ability to polarize and be polarized by the solvent. At the same time, the intrinsic sensitivity of its shielding to such changes in electronic environment is dependent on the factor $<a_0^3/r^3>$. Of course, this is not a unique correlation, and in fact the authors[174] had previously proposed a proportionality to the diamagnetic shielding σ^d of the rare gas atom, although it is not obvious why such a correlation should exist since it is the paramagnetic term that is largely responsible for the deshielding effects of intermolecular interactions for the rare gas atoms.[23] The chemical shift ranges of Xe:Kr:Ne:He in the set of solvents are 250:140:15:0.78.[176] With the same solvents ^{13}C in CH_4 has a relative sensitivity of 9.

4. APPLICATIONS TO MORE COMPLEX SYSTEMS

4.1. Separation of short-range and long-range effects on shielding

Disk space, memory size and computation time often limit the size of the molecule that one can study using *ab initio* methods. During the past few years, nuclear magnetic shielding calculations gained considerable momentum from the developments in both hardware and software. For example, shielding calculations for a molecule with 50 atoms or more are now possible on workstations through direct algorithms.[177–179] With faster processors, the time needed for evaluating two-electron integrals has significantly decreased, rendering the storage of these integrals no longer necessary. Current work in parallelization of code[179] which allows for sharing of computer resources would further ameliorate the present limitations. Simultaneous with these algorithmic advances is the evolution of techniques designed to lessen the computational requirements. The introduction of local origins in the GIAO, IGLO and LORG methods has considerably decreased the saturated basis set size to a manageable level. In addition, the local nature of chemical shielding permitted the use of attenuated basis sets[180] in which only the nucleus of interest and its immediate neighbours are assigned a large number of basis functions. On the other hand, in common origin calculations, it has been observed[181] that a monotonic basis set dependence of the shielding could be established in a small model molecular fragment as in the molecule benzene. Calculations for molecules that are much larger but still similar to benzene (e.g. fullerenes) can then be performed with small basis sets and later extrapolated to the infinite basis size value using the basis set dependence found in benzene. Clearly, the use of physical insight drawn from *ab initio* calculations on small molecules can indeed help in devising strategies to overcome the present practical limitations.

An understanding of the nature and origins of the chemical shift permits categorization and, in turn, can make the computation more manageable. For example, the shielding at a particular nucleus can be subdivided into the following contributions:[65]

$$\sigma_{\text{total}} = \sigma_s + \sigma_l + \sigma_o. \tag{11}$$

The first term, σ_s, represents the short-range contributions to the shielding. In this first term, local structural factors such as bond lengths, bond angles and torsion angles are taken into account. Their evaluation requires full *ab initio* calculations; that is, all atoms contributing to the chemical shift are assigned basis functions and this aspect distinguishes σ_s from the rest of the terms in Eq. (11). Since the categorization is an operational one, interactions other than those arising from changes in the local geometry around the nucleus of interest that likewise needs a full *ab initio* treatment are also

included in σ_s. Examples are intermolecular interactions that occur at shorter distances (< 2.5 Å) and these can either be attractive as in hydrogen bonding[52,71,182] or repulsive as in molecules colliding in the gas phase.[24]

The second term, σ_l, representing the long-range electrostatic contribution, arises from polarization of the electron clouds around the nucleus concerned. Having a relevant range of distances that is much longer than in σ_s, σ_l can be evaluated through a variety of methods. A reaction field could be used. This represents all the atoms not included in σ_s by a uniform dielectric medium. The disadvantage of this approach is that the environment is treated with a strictly non-atomistic model so that differences in configurations of atoms providing the environment outside of σ_s cannot be taken into account at all. A better approach is to replace all other atoms not included in σ_s by point charges or by point electric multipoles, and then calculate the long-range contributions to the shielding due to these point charges and/or multipoles. One method to do this is the charge-field perturbation (CFP) method which is a full *ab initio* treatment of the fragment that includes all atoms participating in σ_s in the presence of the point charges. This method has been shown[65] to give results that compare favourably with supermolecule calculations. Figure 21 exemplifies this favourable agreement in the system where fluorobenzene interacts with hydrogen fluoride. It can be seen that the results obtained using point charges to represent the perturbing HF molecule are very close to the values obtained when basis sets are also assigned to the HF molecule. This approach, the CFP method, can actually be regarded as an extreme case of the locally dense basis technique introduced by Chesnut and Moore.[180] Another method is to do *ab initio* calculations of the fragment (that includes all atoms participating in σ_s) in the presence of a uniform field at various strengths[82] to obtain the shielding polarizabilities defined in Eq. (1) and in an electric field gradient to obtain the shielding derivatives with respect to a field gradient. Alternatively, all these derivatives can be obtained at the same time by Derivative Hartree–Fock (DHF) theory.[183] The Taylor series expansion Eq. (1) plus the gradient terms proposed by Buckingham and Lawley[80] then provide the shielding under any conditions of perturbing electric fields. Only the coefficients in Eq. (1) require *ab initio* methods. Hence, this method offers a fast evaluation of the electrostatic contribution to the shielding provided that the derivatives are already known and only the perturbing electric field needs to be computed classically from point charges or permanent electric multipoles. Shielding polarizabilities and hyperpolarizabilities are now available for a considerable number of small molecules.[81–88] Interestingly, the derivatives calculated for small molecules are also found to be suitable for larger but related systems. As an example, using the ^{19}F shielding polarizabilities in fluorobenzene, the observed ^{19}F shielding inequivalencies in the 5-F-tryptophan-labelled galactose-binding protein (GBP) can be satisfactorily reproduced.[52,184] A recent study shows

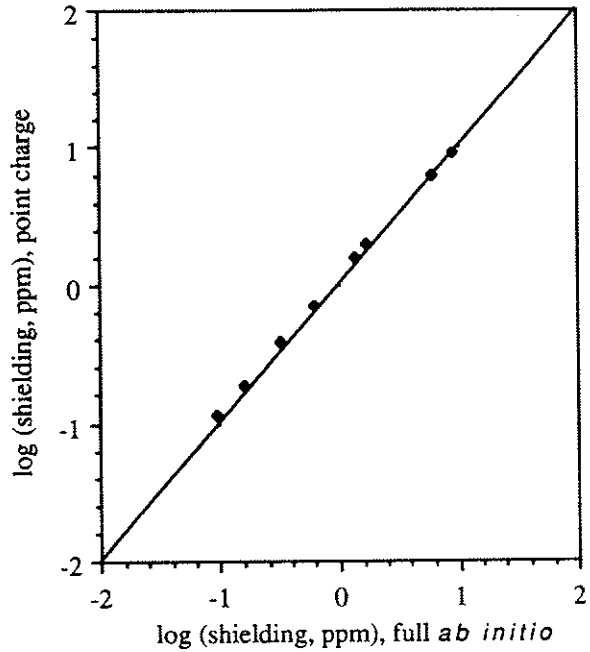

Fig. 21. Chemical shieldings of F in fluorobenzene in a series of C_6H_5F–HF dimers calculated using a full *ab initio* method versus shieldings computed using point charges to represent the HF molecule, as a function of separation distance (r = 2.5→20 Å). Reproduced from Ref. 65, with permission.

that it is in fact necessary to include hypergradient terms in evaluating long-range electrostatic contributions to shielding.[81] Unlike the shielding polarizability approach, the charge-field perturbation method does not rely on the convergence behaviour of the Taylor series expansion in Eq. (1). Representation of all atoms outside of σ_s with point charges resembles closely the non-uniformity of the electric field found in real systems.

The last term in Eq. (11), σ_o, consists of magnetic effects arising from bulk susceptibility, ring-current effects and anisotropy of functional groups such as C=O. Since this contribution to the shielding is due to a variation of the local magnetic field at the site of the nucleus, σ_o is independent of the identity of the nucleus. Consequently, for nuclei other than hydrogen, this term becomes significantly smaller than σ_s and σ_l combined and, at the present level of accuracy of *ab initio* methods, σ_o is still well within the error margin (~ 1 ppm) and, thus, can be neglected.

4.2. Use of scaling and additivity

In addition to having methods that are specialized for a particular shielding contribution, the categorization also allows for the determination of which terms are dominant. And for each of these elements, strategies can be drawn to overcome computational limitations. For example, although the determination of the shielding dependence on internuclear separation has recently become routine, systems involving heavier elements (beyond the third row of the Periods Table) still pose significant computational difficulties. Furthermore, the presence of more than two interacting bodies as observed in real systems can considerably increase the size of the computation. The previous work on Xe systems[24] addresses both these problems by employing scaling and additivity. Using Ar as a model, the shielding behaviour of ^{129}Xe in the gas phase, in solution or as adsorbed species, has been well explained. The scheme involves a scaling procedure similar to what is employed at long range in potential functions[29] except for an additional factor, $<a_0^3/r^3>$ of the ground electronic state of the atom, which takes into account the sensitivity of its shielding to electronic perturbations.[62,63] Thus, from the internuclear dependence of the Ar shielding in the system Ar–Ar, the corresponding shielding functions for Xe–Ar, Xe–Kr and Xe–Xe, for example, can be obtained. Also, the applicability of the functions derived by this scaling procedure to real systems has been verified[24] in reproducing the temperature-dependent second virial coefficients of chemical shielding measured in the gas phase.[156,158] Thus, the presence of scaling factors can be utilized in studying the shielding behaviour of heavier elements. Since *ab initio* calculations are performed on lighter atoms, large basis sets can be used and even inclusion of second-order correlation effects is possible. This is certainly the case for ^{39}Ar in Ar_2 where the second-order LORG (SOLO) method of Bouman and Hansen[6] with a McLean–Chandler 6-311G basis augmented with three sets of *d*-type polarization functions[185] can be accomplished without any difficulty. And from this model study, the conclusion that second-order correlation contributions to shielding are negligible was reached,[24] an observation that is certainly much more difficult to gather for ^{129}Xe.

Real systems, especially in condensed phase, consist of more than a pair of interacting atoms or molecules. The question of how applicable the shielding functions of two-atom systems are to larger clusters comes into the picture. Calculations of ^{39}Ar shielding in argon clusters[24] indicate that there is additivity; that is, the intermolecular shielding of the central Ar atom in a linear Ar_3 cluster with interatomic distances of R is equivalent to twice that of an Ar_2 dimer separated by the same distance R. And using this additivity, a successful quantitative prediction of the ^{129}Xe chemical shifts of Xe, Xe_2 up to Xe_8 trapped in cages of zeolite NaA has been achieved.[102] Likewise, it should be of no surprise to see that the long-range electrostatic effects are also additive.[65] However, caution should be exercised, for the additivity breaks down at some distances depending on the type of interaction present. For interacting pairs of rare gas atoms, the importance of three-body terms starts to appear only at separations well inside the repulsive regions. And in the case of long-range electrostatic effects, mutual polarizations seem to be unimportant as long as the distances of interactions are longer than 2.5 Å.

The presence of scaling factors is not exclusive to an interacting pair of rare gas atoms. At much shorter distances and stronger interactions, as in the vicinity of the equilibrium bond length in diatomic hydrides, a similar relationship exists.[23] The Cl and F shieldings over the range of bond lengths within the classical turning-points of the ground vibrational states of HCl and HF are made superposable upon scaling by the factors $<a_0^3/r^3>R_e$, where R_e is the equilibrium bond length. This appears to be true as well for ClF and F_2. Even with the alkali hydrides, as in ^{23}Na in NaH and ^{7}Li in LiH, although less ideal, the scaling still seems to work. Furthermore, it is unlikely that this relationship is restricted to diatomics especially when the first hints of the $<a_0^3/r^3>$ dependence of the internuclear shielding traces originated from studies of ^{15}N in NH_3 and ^{31}P in PH_3.[32,33] However, the scaling holds only in a narrow range. In diatomic molecules, beyond the turning-points of the ground vibrational state, the breakdown is already imminent.

The additivity of contributions to the shielding originates from their separability from each other. It may even be possible to consider separate contributions to the short-range part: local geometry factors, hydrogen bonding and repulsive orbital overlap contributions. The local geometry factors can be evaluated separately into bond length, bond angle and dihedral angle effects. This separability manifests itself in the relatively lower magnitudes of the mixed shielding derivatives. And as deduced from *ab initio* calculations of shielding traces for ^{15}N in NH_3[32] and ^{31}P in PH_3,[33] the mixed derivative of the shielding with respect to simultaneous changes in bond length and bond angle is negligibly small at the equilibrium geometry. Furthermore, the mixed terms contribute only very little to the rovibrational corrections at 300 K for these molecules. The universal additivity of isotope shifts is a consequence of the very small mixed derivatives of shielding with respect to different stretches, stretch and angle deformation, stretch and torsion, etc. Separability enables the recognition of which factors contribute the most. For example, analysis of the various contributions to ground-state vibrational corrections for the shielding of the heavy atom in the following hydrides: H_2O,[30] CH_4,[117] NH_3[32] and PH_3,[33] reveals that bond length effects are dominant. Likewise, the dominance of the bond length contribution is also evident in the secondary deuterium isotope shifts.

The above observations are not exclusive to the shielding surfaces of simple hydrides. Molecules as complex as amino acid derivatives also exhibit the separability of the short-range contributions to the shielding into bond

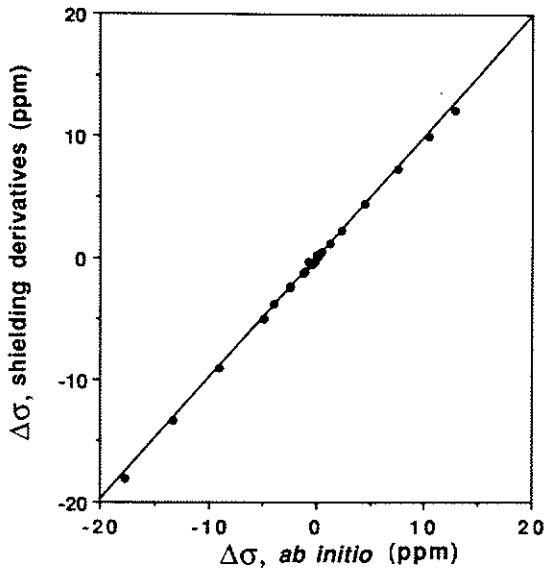

Fig. 22. Effects of simultaneously varying C^{α}–N and C^{α}–C^{O} bond lengths on the C^{α} shielding, calculated using a full *ab initio* treatment (horizontal axis) or using the bond length shielding derivatives (vertical axis). Reproduced from Ref. 41, with permission. Copyright 1993, American Chemical Society.

length, bond angle and torsion angle effects.[41] Figure 22 shows the separability of the C^{α}–N and C^{α}–C^{O} bond length effects on the C^{α} shielding in formyl-L-alanine amide. It is clear that in this case, based on the excellent agreement between full *ab initio* treatment and individual shielding derivative treatment, the bond effects are additive and can be evaluated separately. This is a very significant finding: that there is no need to calculate complete shielding hypersurfaces since individual traces apparently suffice. Figure 23 shows the separability of bond length effects from the torsion angle contributions. Bond lengths normally do not vary too much, thus, traces that cover a range of 0.2 Å are more than adequate. On the other hand, the range of torsion angles observed for amino acid residues in proteins covers a significant region of the whole space. In Figure 23, it can be seen that even with large changes in torsion angles, the shielding dependence on the bond length is unchanged. Thus, in this particular case, there is enough confidence that a shielding trace with respect to bond length changes evaluated at specific torsion angles is equally valid for other torsion angles. Determining beforehand the contributions that can be treated individually can greatly reduce the computational effort required. Unfortunately, separability does not hold for all internal coordinates. For example,

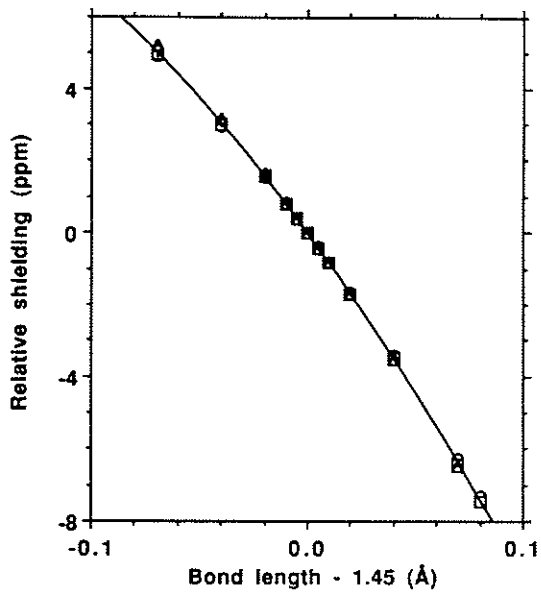

Fig. 23. Alanine C^{α} shielding as a function of the C^{α}–N bond length at different ϕ and ψ angles: helix ($\phi = -58$, $\psi = -51$) (○), turn ($\phi = 55$, $\psi = 50$) (△), and sheet ($\phi = -71$, $\psi = 140$) (□). Reproduced from Ref. 41, with permission. Copyright 1993, American Chemical Society.

the huge range of values of backbone torsion angles ϕ and ψ observed in proteins precludes the use of individual torsion angle shielding traces. Moreover, in other amino acids where the side-chain is more complicated than that of alanine, an additional torsion angle, χ^1, needs consideration. This demands computation of shielding hypersurfaces that takes into account ϕ, ψ and χ^1 effects.[50]

The assumption of separability of contributions to shielding combined with *ab initio* calculations of model fragments has permitted leaps in the progress in our understanding of the chemical shift in complex systems. Although chemical shift inequivalencies in protein NMR have been observed for some time,[186–188] the long-awaited explanation for the origins of such inequivalencies became evident only recently via partitioning of the shielding contributions.[41,42,50–52,65] In these studies, the dominant factors that cause the range of chemical shifts of ^{13}C, ^{15}N and ^{19}F in proteins have been identified. The differences observed in C^{α} shielding of alanine sites in proteins have been mainly attributed to the backbone torsion angles ϕ and ψ.[41, 50–52] The C^{β} shielding, on the other hand, in addition to its sensitivity to the torsion angles, is also influenced by long-range electrostatic factors.[50] In both cases, C^{α} and C^{β}, it would have been impossible to reproduce the

experimentally observed trends using *ab initio* methods by simply using coordinates directly obtained from an X-ray structure. The large spread of values in bond lengths for the same type of residue in a single protein leads to calculated chemical shielding values that correlate with neither the range nor the pattern of observed shifts. Knowing how sensitive the chemical shielding is to bond length variations and comparing the experimentally observed shift range with the values one would obtain from the bond lengths directly extracted from an X-ray structure, it has become apparent that the variations in bond lengths presently found in X-ray structures cannot be reconciled with chemical shift range and trends. On the other hand, by simply taking into account the contributions arising from torsion angles, one can, in fact, reproduce quite well the observed C^{α} chemical shifts in proteins.[51] The nucleus ^{19}F, although not naturally occurring in proteins, serves as an excellent probe for studying electrostatic effects on the chemical shift. Being an atom that sits on the periphery and having a substantial shielding polarizability,[184] the fluorine shielding inequivalencies observed in ^{19}F-tryptophan-labelled proteins can be expected to be dominated by long-range electrostatic factors. And it has been shown that the experimentally observed trend for ^{19}F NMR in proteins can be reproduced by using either a charge-field perturbation[52] or the shielding polarizability approach.[184] Lastly, ^{15}N chemical shifts prove to be the most complicated. The short-range factors now include not only the torsion angles, ϕ, ψ and χ^1 of the residue which carries that ^{15}N nucleus of interest but also the torsion angles of the preceding residue.[52–53] To further complicate the situation, hydrogen bonding and long-range electrostatic effects are also important.[52] However, as long as one can take into account all of these factors, a quantitative prediction of the ^{15}N chemical shifts in proteins is still possible. In addition, it is noteworthy to point out that some of the contributions to ^{15}N chemical shifts are separable, indicating that some of these can be evaluated individually[52] if computer resources prevent a full *ab initio* treatment.

Indeed, by separating the contributions to chemical shielding and taking advantage of their additivities, complicated systems ranging from species adsorbed in zeolite cages to large molecules such as proteins become tractable even with limited computer resources.

4.3. Use of electric field effects and dynamic averaging

As mentioned earlier, the time period of an NMR measurement allows for sampling over various conformations. Motions that are faster than the NMR time scale result in an averaging of the shielding in all three contributions: short-range, long-range and magnetic effects. The extent and significance of the dynamic averaging in each of these contributions depend on their

sensitivity to such motions. As seen in small molecules,[30,32,33,117] ground-state vibrational corrections to the shielding are largely due to bond stretching. Of course, upon seeing how dramatic the shielding changes with variations in bond lengths, this observation should come as no surprise at all. The relative importance of motional averaging in each of the contributions also depends on which trend in experimental chemical shifts is of interest. Although the contributions of bond angle changes to the ground-state vibrational corrections are less than substantial, when it comes to the temperature dependence of the chemical shift in isolated molecules, bending motions and internal rotations begin acquiring active roles. The magnitude of the motional sampling evidently depends on the amplitude of such motion, and the shape of the potential surface dictates this amplitude. Thus, dynamic averaging of the shielding involves two surfaces: the shielding surface, this describes how shielding changes with motion; and the potential surface, this governs which configurations are possible and which ones are sampled most often. Invoking a categorization of the dynamic averaging of the shielding into various short-range effects and long-range electrostatic contributions therefore faces additional complications. The question arises, for example, of how motions involving changes in the local geometry around the nucleus affect its shielding polarizability. Separability does not apply if the motions cannot be treated individually. Fortunately, there are some cases wherein the system allows for such separation.

Thus, before one steps into more complicated systems, it is necessary to begin with systems that can serve as tests specific for a particular contribution. This has been one of the primary aims of the Jameson group and other laboratories such as Raynes', evident in their long list of chemical shift measurements in the gas phase [see Ref. 101 and references therein]. Through chemical shift measurements at various densities and temperatures in the gas phase, data that involve only the dynamic averaging of collision effects (σ_1 and its temperature dependence) or data that pertain only to the isolated molecule (rovibrational effects) can be obtained. And with these numbers available, the gauging of computational strategies designed to evaluate a particular contribution to shielding has been made possible. The shielding of rare gas atoms provides an excellent case for studying the averaging of collision effects on shielding. The excellent agreement between calculated and experimental σ_1 values for ^{129}Xe provides a strong indication that the scaling of interatomic shielding traces for rare gas atoms is a working procedure.[24] The successful quantitative prediction of the ^{129}Xe chemical shifts in Xe adsorbed in the alpha cages of zeolite NaA as a function of cluster size and temperature strongly supports the additivity of environmental effects to shielding.[102] And for contributions arising from bond length and bond angle changes, the works on ^{13}C in CH_4,[117] ^{15}N in NH_3,[32] and ^{31}P in PH_3[33] offer convincing support for current rovibrational averaging methods.

Incorporation of dynamics has not been limited to small systems. The first successful attempt in reproducing chemical shifts in proteins that includes effects of motional averaging has already been reported.[184] This case illustrates an example wherein one factor, long-range electrostatics, dominates. By combining shielding polarizabilities, how the shielding tensor elements respond to the uniform field components and their gradient terms, with the values of the fields and field gradients obtained from molecular dynamics, a series of "shielding trajectories" can be generated. In this work, the results greatly depend on how adequate current force fields for proteins are, and, in particular, on how precise methods of computing protein electrostatics are. The Local Reaction Field model and the protein atomic charge set employed in the current ENZYMIZ program of Lee *et al.*[189] appear to be useful in generating long-range electrostatic "shielding trajectories" that can explain experimental trends. One special feature of this charge set is that the sum of the atomic charges of all side-chains is zero. The absence of ionized groups apparently accounts for the insensitivity of the chemical shift to charged surface side-chains, as observed in experiment.[190] However, since this study involves only ^{19}F chemical shifts in proteins in which long-range electrostatic contributions dominate, general conclusions regarding the construction of "shielding trajectories" should be drawn with caution. In this special case, the most crucial part of the computation is the evaluation of electrostatic terms. In order to verify the rest of protein force fields that describe stretches, bendings and internal rotations, nuclear shielding that exhibits sensitivity to short-range effects needs to be considered. In this respect the C^α and C^β nuclei are excellent candidates. Since the range of the torsion angles ϕ, ψ and χ^1 observed in proteins prohibits the use of shielding traces, the fastest way to evaluate the shielding at any given set of torsion angles requires shielding surfaces or even hypersurfaces. Thus, shielding surfaces serving as look-up tables for torsion angle effects, combined with shielding traces expressed as Taylor expansions that enable fast evaluation of bond length and bond angle changes, plus the use of shielding polarizabilities, provide an excellent route for incorporating molecular dynamics into protein chemical shift calculations. The strategy is certainly conceivable; however, the accuracy of the shielding surfaces still requires validation.

4.4. Predicting shifts in complex systems from shielding surfaces of model systems

As mentioned earlier in this review, it has been demonstrated that using coordinates from relaxed X-ray structures of proteins (where the large variations in bond lengths have been removed),[52] the observed chemical shift inequivalencies in protein NMR spectroscopy can be quantitatively

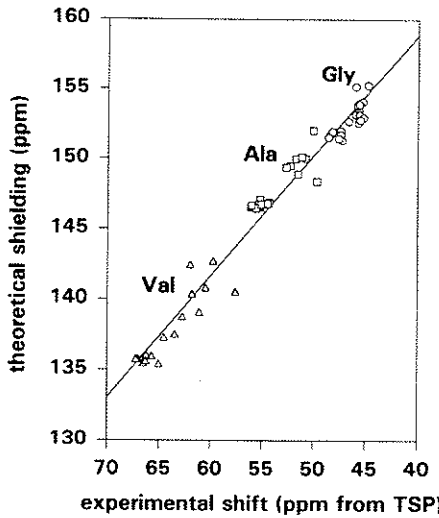

Fig. 24. Theoretical C^α shieldings extracted from ϕ–ψ surfaces versus experimental C^α shifts in glycine, alanine and valine residues of calmodulin and SNase. Reproduced from Ref. 51.

predicted using *ab initio* methods. In addition, it is already known that the chemical shift dispersion seen in C^α resonances for a given residue is mainly due to differences in the torsion angles ϕ, ψ and χ^1.[41,42] The C^α chemical shifts in proteins can therefore serve as a gauge for evaluating the accuracy of torsion angle shielding surfaces.

Influences of the torsion angle on the chemical shift are considered short range. Hence, a molecular model fragment that resembles a particular amino acid residue in its ϕ, ψ and χ^1 angles should be adequate in constructing the shielding surfaces. Model compounds in the form of *N*-formyl-L-amino acid amide have been used, for example, to describe the torsion angle effects on the C^α shielding in glycine, alanine and valine residues.[41,50,51] One example of these surfaces (alanine) was shown in Fig. 7. Using the shielding surfaces derived from the small model compounds and the torsion angles extracted from X-ray structures of the proteins Vertebrae calmodulin[191] and staphylococcal nuclease (SNase),[192] the pattern observed for the C^α chemical shifts in glycine, alanine and valine residues of this protein is well reproduced[51] as shown in Fig. 24. The r.m.s.d. of the points from the fitted curve is only 1.0 ppm and the slope of the line in 0.9. The good correlation between theory and experiment seen from a total of 57 points derived from two proteins convincingly manifests the usefulness of the torsion angle shielding surfaces determined from small model fragments and the dominance of the short-range contributions. A similar situation

exists in C^β shifts, although less ideal than in C^α. The difficulty in quantitatively reproducing C^β shifts is not due to inaccuracy of the shielding surfaces but to the long-range electrostatic effects becoming significant for the shielding of these nuclei.[50]

Thus, there is sufficient indication that generating "shielding trajectories" which take into account not only the dynamic averaging of long-range electrostatic effects but also bond length, bond angle and torsion angle effects is feasible. The success in interpreting experimental results using shielding trajectories, however, relies on factors other than the applicability of shielding traces, surfaces and polarizabilities. The shielding surface is only half the picture of dynamic averaging. The other half is the potential surface. How adequate are the potential surfaces in use now? Based on preliminary results, there is indication that model force fields currently available may not be generally applicable for this purpose. For example, relaxation by steepest descent in 2000 steps of the protein X-ray structure using the AMBER[193] force field worsens the correlation between calculated shieldings and experimental shifts for the C^α site in glycine residues in the two proteins, calmodulin and SNase.[42,51] On the other hand, both C^α and C^β shieldings in the alanine residues benefit from the minimization of the X-ray structure. This means that the force field leads to a minimum energy configuration that is not good enough to provide internally consistent chemical shifts to within NMR experimental accuracy. The NMR chemical shift provides an additional observable to help in studying protein mechanics and dynamics.

Lastly, the goal of theoretical studies of the chemical shielding is not simply to reproduce experimentally observed chemical shifts. By separating the various contributions to the chemical shift, a powerful tool in analysing structure and dynamics can be realized. The contributions, whether short range as in bond lengths, bond angles or torsion angles, hydrogen-bonding or non-bonded overlap, or long-range electrostatic, are of great interest for their own sake, and knowing how to relate the observed chemical shift to these factors is indeed a powerful tool in studying complex systems. For example, the ability to predict ^{129}Xe chemical shifts of the xenon clusters trapped inside cages of zeolite NaA has significantly contributed to our understanding of the nature of these clusters.[102] The chemical shifts and their temperature dependence have shown how valid Grand Canonical Monte-Carlo methods are in describing the dynamics of xenon atoms inside zeolite cages. With the analysis of the origins of chemical shift inequivalencies in proteins, it is now known that bond lengths in proteins are more uniform than what present X-ray structures provide. More importantly, the dominance of torsion angle effects in backbone ^{13}C shifts has opened a new route in predicting and refining protein structure. A well-defined relationship between the torsion angles and chemical shielding allows for extracting secondary structure information from measured NMR chemical

shifts. Oldfield and coworkers have already taken advantage of this relationship by employing what they call a Z-surface,[51] a probability function that gives the most likely values of the angles ϕ and ψ given a measured chemical shift:

$$Z_i(\phi, \psi) = \exp - \left\{ \frac{P_i - f_i(\phi, \psi)}{W_i} \right\}^2 \tag{13}$$

This equation, not exclusive to chemical shifts but applicable to other observables, compares the experimental value of property P_i with that obtained from either an empirical or *ab initio* surface f_i. A good match, for example, between the calculated shielding surface and the observed chemical shift leads to a large value of Z. The whole torsion angle space can then be explored and, at the end, regions represented by Gaussians having width W_i (standard deviation derived from a comparison between experimental values and those obtained from the surface in a system with known structure) reflecting the most probable ϕ and ψ pairs of values are obtained. Individual Z-surfaces obtained from independent observables that are functions of the same ϕ and ψ angles, such as chemical shifts of other nuclei in the same residue or spin–spin coupling constants, can be combined until one has narrowed down the non-zero areas of the Z-surface into a unique solution of ϕ and ψ angles. Preliminary studies have shown that, with this approach, values for ϕ and ψ are obtained within 10° from their X-ray values.[51]

5. CONCLUSIONS

The NMR chemical shift serves as a paradigm for the effects of intramolecular dynamics and intermolecular interactions on molecular electronic properties. Details of the property surface, its dependence on internuclear distances, bond angles, and torsion angles, its response to electric fields and electric field gradients, have been explored to a greater extent than any other molecular electronic property. The rovibrational averaging on this surface leads to the observed temperature dependence in the gas at the zero-pressure limit and the mass dependence in the vast number of observed isotope shifts. Averaging over the intermolecular collisions in a dilute gas leads to the observed temperature-dependent virial coefficients of this property, again serving as an example for other properties. It has become clear that only a proper dynamic averaging over the intermolecular shielding surface can account for the virial coefficients, their dependence on temperature and on the nuclear site. Averaging the shielding function in a grand canonical ensemble for an inhomogeneous fluid inside the pores of a zeolite

leads to the observed temperature-dependent average chemical shifts of the trapped clusters in zeolite pores containing one, or two, up to eight atoms. The combination of the ultra-high-resolution measurements with the nuclear site specificity of the NMR chemical shift and the feasibility of *ab initio* quantum mechanical calculations has permitted the exploration of this electronic property surface and dynamic averaging on it. The remaining challenges, in addition to relativistic and electron-correlated *ab initio* computations of shielding surfaces to include heavy nuclei such as those of transition metal elements and post-transition nuclei, appear to be in the proper treatment of extended networks. At the present time, only small fragments of such networks have been treated quantum-mechanically, such as the $[SiO_4]^{-4}$ unit to represent silicates. Approaches to complex systems such as proteins that have been developed provide new insight into the interdependence of shielding and structure. However, other systems such as ionic and covalent solids have so far been treated only at the empirical level. Although the NMR chemical shift tensors in these solids have been used as tools for characterization, a level of theory such as has been described in this review has not yet proved feasible.

ACKNOWLEDGEMENT

CJJ is grateful for the continuing support of the National Science Foundation (Grant CHE92-10790).

REFERENCES

1. R. M. Stevens, R. M. Pitzer and W. N. Lipscomb, *J. Chem. Phys.*, 1963, **38**, 550.
2. P. Lazzeretti and R. Zanasi, *J. Chem. Phys.*, 1978, **68**, 1523.
3. J. Oddershede, P. Jorgensen and D. L. Yeager, *Comput. Phys. Rep.*, 1984, **2**, 33.
4. D. M. Bishop and S. M. Cybulski, *J. Chem. Phys.*, 1993, **98**, 8057.
5. A. E. Hansen and T. D. Bouman, *J. Chem. Phys.*, 1985, **82**, 5035.
6. T. D. Bouman and A. E. Hansen, *Chem. Phys. Lett.*, 1990, **175**, 292.
7. M. Schindler and W. Kutzelnigg, *J. Chem. Phys.*, 1982, **76**, 1919.
8. C. van Wüllen and W. Kutzelnigg, *Chem. Phys. Lett.*, 1993, **205**, 563.
9. R. Ditchfield, *Mol. Phys.*, 1974, **27**, 789.
10. K. Wolinski, J. Hinton and P. Pulay, *J. Am. Chem. Soc.*, 1990, **112**, 8251.
11. J. Gauss, *Chem. Phys. Lett.*, 1992, **191**, 614.
12. D. B. Chesnut, *Annual Reports on NMR Spectroscopy*, ed. G. A. Webb, Academic Press, London, 1994, pp. 71–122, this volume.
13. C. J. Jameson and A. C. de Dios, in *Nuclear Magnetic Shieldings and Molecular Structure*, ed. J. A. Tossell, NATO ASI Series C Vol. 386, Kluwer, Dordrecht, 1993, pp. 95–116.
14. R. A. Hegstrom, *Phys. Rev. A*, 1979, **19**, 17.
15. R. M. Stevens and W. N. Lipscomb, *J. Chem. Phys.*, 1964, **40**, 2238.
16. R. M. Stevens and W. N. Lipscomb, *J. Chem. Phys.*, 1964, **41**, 184.

17. R. M. Stevens and M. Karplus, *J. Chem. Phys.*, 1968, **49**, 1094.
18. E. A. Laws, R. M. Stevens and W. N. Lipscomb, *J. Chem. Phys.*, 1971, **54**, 4269.
19. R. Ditchfield, *Chem. Phys.*, 1981, **63**, 185.
20. D. B. Chesnut, *Chem. Phys.*, 1986, **110**, 415.
21. D. B. Chesnut and C. K. Foley, *J. Chem. Phys.*, 1986, **85**, 2814.
22. D. B. Chesnut and C. K. Foley, *J. Chem. Phys.*, 1986, **84**, 852.
23. C. J. Jameson and A. C. de Dios, *J. Chem. Phys.*, 1993, **98**, 2208.
24. C. J. Jameson and A. C. de Dios, *J. Chem. Phys.*, 1992, **97**, 417.
25. RPAC, T. D. Bouman, Southern Illinois University, Edwardsville, and A. E. Hansen, H. C. Oersted Institute, Copenhagen, Denmark.
26. H. Wind, *J. Chem. Phys.*, 1965, **42**, 2371; 1965, **43**, 2956.
27. M. Giroud and O. Nedelec, *J. Chem. Phys.*, 1980, **73**, 4151.
28. L. A. Viehland, *Chem. Phys.*, 1984, **85**, 291.
29. G. C. Maitland, M. Rigby, E. B. Smith and W. A. Wakeham, *Intermolecular Forces, Their Origin and Determination*, Clarendon, Oxford, 1981.
30. P. W. Fowler, G. Riley and W. T. Raynes, *Mol. Phys.*, 1981, **42**, 1463.
31. P. Lazzeretti, R. Zanasi, A. J. Sadlej and W. T. Raynes, *Mol. Phys.*, 1987, **62**, 605.
32. C. J. Jameson, A. C. de Dios and A. K. Jameson, *J. Chem. Phys.*, 1991, **95**, 1069.
33. C. J. Jameson, A. C. de Dios and A. K. Jameson, *J. Chem. Phys.*, 1991, **95**, 9042.
34. J. A. Tossell and P. Lazzeretti, *J. Magn. Reson.*, 1988, **80**, 39.
35. D. B. Chesnut and D. W. Wright, *J. Comput. Chem.*, 1991, **12**, 546.
36. C. J. Jameson, *J. Chem. Phys.*, 1977, **66**, 4977.
37. C. J. Jameson, *J. Chem. Phys.*, 1977, **66**, 4983.
38. C. J. Jameson, *Mol. Phys.*, 1985, **54**, 73.
39. C. J. Jameson and H. J. Osten, *J. Am. Chem. Soc.*, 1985, **107**, 4158.
40. C. J. Jameson and H.-J. Osten, *Ann. Rept NMR Spectrosc.*, 1986, **17**, 1.
41. A. C. de Dios, J. G. Pearson and E. Oldfield, *J. Am. Chem. Soc.*, 1993, **115**, 9768.
42. D. D. Laws, A. C. de Dios and E. Oldfield, *J. Biomol. NMR*, 1993, **3**, 607.
43. E. G. Paul and D. M. Grant, *J. Am. Chem. Soc.*, 1963, **85**, 1701.
44. F. A. L. Anet and A. K. Cheng, *J. Am. Chem. Soc.*, 1975, **97**, 2420.
45. H. Kurosu, I. Ando and G. A. Webb, *Magn. Reson. Chem.*, 1993, **31**, 399.
46. D. B. Chesnut, D. W. Wright and R. A. MacPhail, *Chem. Phys. Lett.*, 1988, **151**, 415.
47. W. Kutzelnigg, C. van Wüllen, U. Fleischer, R. Franke, and T. van Mourik, in *Nuclear Magnetic Shieldings and Molecular Structure*, ed. J. A. Tossell, NATO ASI Series C Vol. 386, Kluwer, Dordrecht, 1993, pp. 141–161.
48. M. Barfield and S. H. Yamamura, *J. Am. Chem. Soc.*, 1990, **112**, 4747
49. M. Barfield, in *Nuclear Magnetic Shieldings and Molecular Structure*, ed. J. A. Tossell, NATO ASI Series C Vol. 386, Kluwer, Dordrecht, 1993, pp. 523–537.
50. A. C. de Dios and E. Oldfield, *J. Am. Chem. Soc.*, 1994, **116**, 5307.
51. J. G. Pearson, H. Le, A. C. de Dios and E. Oldfield, *J. Am. Chem. Soc.*, in press.
52. A. C. de Dios, J. G. Pearson and E. Oldfield, *Science*, 1993, **260**, 1491.
53. H. Le and E. Oldfield, *J. Biomol. NMR*, 1994, **4**, 341
54. S. Spera and A. Bax, *J. Am. Chem. Soc.*, 1991, **113**, 5490.
55. C. J. Jameson and H. J. Osten, *J. Chem. Phys.*, 1984, **81**, 4293.
56. C. J. Jameson, in *Isotopes in the Physical and Biomedical Sciences*, ed. E. Buncel and J. R. Jones, Vol. 2 Isotopic Applications in NMR Studies, Elsevier, Amsterdam, 1991, pp. 1–54.
57. S. F. Boys and F. Bernardi, *Mol. Phys.*, 1970, **19**, 553.
58. C. J. Jameson, *J. Chem. Phys.*, 1975, **63**, 5296.
59. C. J. Grayce and R. A. Harris, *Mol. Phys.*, 1991, **72**, 523.
60. T. W. Marshall and J. A. Pople, *Mol. Phys.*, 1960, **3**, 339.
61. J. P. Riley, I. H. Hillier and W. T. Raynes, *Mol. Phys.*, 1979, **38**, 353.
62. C. J. Jameson and H. S. Gutowsky, *J. Chem. Phys.*, 1964, **40**, 1714.

63. C. J. Jameson and J. Mason in *Multinuclear Nuclear Magnetic Resonance*, ed. J. Mason, Plenum Press, London, 1987, pp. 51–88.
64. C. J. Jameson, A. K. Jameson, R. E. Gerald II and A. C. de Dios *J. Chem. Phys.*, 1992, **96**, 1676.
65. A. C. de Dios and E. Oldfield, *Chem. Phys. Lett.*, 1993, **205**, 108.
66. R. Ditchfield, *Chem. Phys.*, 1981, **63**, 185.
67. D. B. Chesnut and C. G. Phung, *Chem. Phys.*, 1990, **147**, 91.
68. J. F. Hinton and D. L. Bennet, *Chem. Phys. Lett.*, 1985, **116**, 292.
69. J. F. Hinton, P. Guthrie, P. Pulay and K. Wolinski, *J. Am. Chem. Soc.*, 1992, **114**, 1604.
70. A. Pines, D. J. Ruben, S. Vega and M. Mehring, *Phys. Rev. Lett.*, 1976, **36**, 110.
71. M. Munch, A. E. Hansen, P. E. Hansen and T. D. Bouman, *Acta Chem. Scand.*, 1992, **46**, 1065.
72. J. C. Christofides and D. B. Davies, *Magn. Reson. Chem.*, 1985, **23**, 582.
73. J. C. Facelli, R. H. Contreras and M. F. Tufro, *J. Mol. Structure* (Theochem), 1993, **281**, 61.
74. D. B. Chesnut and C. G. Phung, in *Nuclear Magnetic Shieldings and Molecular Structure*, ed. J. A. Tossell, NATO ASI Series C Vol. 386, Kluwer, Dordrecht, 1993, pp. 221–243.
75. M. J. Stephen, *Mol. Phys.*, 1958, **1**, 223.
76. A. D. Buckingham, *Can. J. Chem.*, 1960, **38**, 300.
77. A. D. Buckingham and S. M. Malm, *Mol. Phys.*, 1971, **22**, 1127.
78. W. T. Raynes and R. Ratcliffe, *Mol. Phys.*, 1979, **37**, 571.
79. J. D. Augspurger, C. E. Dykstra and E. Oldfield, *J. Am. Chem. Soc.*, 1991, **113**, 2447.
80. A. D. Buckingham and K. P. Lawley, *Mol. Phys.*, 1960, **3**, 219.
81. J. D. Augspurger, A. C. de Dios, E. Oldfield and C. E. Dykstra, *Chem. Phys. Lett.*, 1993, **213**, 211.
82. M. J. Packer and W. T. Raynes, *Mol. Phys.*, 1990, **69**, 391.
83. W. T. Raynes, in *Nuclear Magnetic Shieldings and Molecular Structure*, ed. J. A. Tossell, NATO ASI Series C Vol. 386, Kluwer, Dordrecht, 1993, pp. 401–420.
84. M. Grayson and W. T. Raynes, *Mol. Phys.*, 1994, **81**, 533.
85. J. D. Augspurger and C. E. Dykstra, *Mol. Phys.*, 1992, **76**, 229.
86. D. M. Bishop and S. M. Cybulski, *Mol. Phys.*, 1993, in press.
87. J. D. Augspurger and C. E. Dykstra, *J. Phys. Chem.*, 1991, **95**, 9230.
88. D. M. Bishop and S. M. Cybulski, *J. Magn. Reson., A*, 1994, **107**, 99.
89. W. T. Raynes, A. D. Buckingham and H. J. Bernstein, *J. Chem. Phys.*, 1961, **36**, 3481.
90. F. London, *Z. Phys. Chem. (Leipzig) B*, 1930, **11**, 222.
91. F. London, *Trans. Faraday Soc.*, 1937, **33**, 8.
92. D. R. Herschbach and V. W. Laurie, *J. Chem. Phys.*, 1961, **35**, 458.
93. J. C. Facelli, A. M. Orendt, M. S. Solum, G. Depke, D. M. Grant and J. Michl, *J. Am. Chem. Soc.*, 1986 **108**, 4268.
94. M. S. Solum, J. C. Facelli, J. Michl and D. M. Grant, *J. Am. Chem. Soc.*, 1986, **108**, 6464.
95. J. C. Facelli, A. M. Orendt, A. J. Beeler, M. S. Solum, G. Depke, K. D. Malsch, J. W. Downing, P. S. Murthy, D. M. Grant and J. Michl, *J. Am. Chem. Soc.*, 1985, **107**, 6749.
96. J. C. Facelli, D. M. Grant and J. Michl, *Acc. Chem. Research*, 1987, **20**, 152.
97. A. M. Orendt, J. C. Facelli, A. J. Beeler, K. Reuter, W. J. Horton, P. Cutts, D. M. Grant and J. Michl, *J. Am. Chem. Soc.*, 1988, **110**, 3386.
98. T. M. Duncan, *A Compilation of Chemical Shift Anisotropies*, Farragut Press, Chicago, 1990.
99. C. J. Jameson, in *Theoretical Models of Chemical Bonding*, ed. Z. B. Maksic, Part 3, Molecular Spectroscopy, Electronic Structure and Intramolecular Interactions, Springer-Verlag, Berlin, 1991, pp. 457–519.
100. G. Riley, W. T. Raynes and P. W. Fowler, *Mol. Phys.*, 1979, **38**, 877.
101. C. J. Jameson, *Chem. Rev.*, 1991, **91**, 1375.

102. C. J. Jameson, A. K. Jameson, B. I. Baello and H. M. Lim, *J. Chem. Phys.*, 1994, **100**, 5965.
103. C. J. Jameson, A. K. Jameson and S. M. Cohen, *J. Chem. Phys.*, 1977, **67**, 2771.
104. A. K. Jameson, K. Schuett, C. J. Jameson and S. M. Cohen, *J. Chem. Phys.*, 1977, **67**, 2821.
105. C. J. Jameson and H. J. Osten, *Mol. Phys.*, 1985, **55**, 383.
106. C. J. Jameson, A. K. Jameson, S. Wille and P. M. Burrell, *J. Chem. Phys.*, 1981, **74**, 853.
107. C. J. Jameson, A. K. Jameson, H. Parker, S. M. Cohen, and C. L. Lee, *J. Chem. Phys.*, 1978, **68**, 2861.
108. C. J. Jameson, A. K. Jameson and H. Parker, *J. Chem. Phys.*, 1978, **69**, 1318.
109. C. J. Jameson, A. K. Jameson and S. Wille, *J. Phys. Chem.*, 1979, **83**, 3372.
110. C. J. Jameson and A. K. Jameson, *J. Magn. Reson.*, 1985, **62**, 209.
111. C. J. Jameson, A. K. Jameson and D. Oppusunggu, *J. Chem. Phys.*, 1985, **83**, 5420.
112. C. J. Jameson, *J. Chem. Phys.*, 1977, **67**, 2814.
113. P. W. Fowler, *Mol. Phys.*, 1981, **46**, 591.
114. C. J. Jameson, *Bull. Magn. Reson.*, 1980, **3**, 3.
115. C. J. Jameson, A. K. Jameson and D. Oppusunggu, *J. Chem. Phys.*, 1986, **85**, 5480.
116. B. Bennett and W. T. Raynes, *Magn. Reson. Chem.*, 1991, **29**, 946.
117. W. T. Raynes, P. W. Fowler, P. Lazzeretti, R. Zanasi and M. Grayson, *Mol. Phys.*, 1988, **64**, 143.
118. P. W. Fowler and W. T. Raynes, *Mol. Phys.*, 1981, **43**, 65.
119. C. J. Jameson, in *Nuclear Magnetic Resonance*, ed. G. A. Webb, Royal Society of Chemistry, London, 1989, Vol. 19, pp. 1–33.
120. J. C. Facelli and D. M. Grant, *Topics Stereochem.*, 1989, **19**, 1.
121. W. T. Raynes and B. Bennett, *Magn. Reson. Chem.*, 1991, **29**, 955.
122. H. Batiz-Hernandez and R. A. Bernheim, *Prog. NMR Spectrosc.*, 1967, **3**, 63.
123. R. E. Wasylishen and J. O. Friedrich, *J. Chem. Phys.*, 1984, **80**, 585.
124. R. E. Wasylishen and J. O. Friedrich, *Can. J. Chem.*, 1987, **65**, 2238.
125. W. Gombler, *J. Am. Chem. Soc.*, 1982, **104**, 6616.
126. P. E. Hansen, *Prog. NMR Spectrosc.*, 1988, **20**, 207.
127. O. Eppers and H. Gunther, *Helv. Chim. Acta*, 1990, **73**, 2071.
128. O. Eppers and H. Gunther, *Helv. Chim. Acta*, 1992, **72**, 2553.
129. W. T. Raynes, *Mol. Phys.*, 1988, **63**, 719.
130. M. Alei and W. E. Wageman, *J. Chem. Phys.*, 1978, **68**, 783.
131. A. K. Jameson and C. J. Jameson, *J. Magn. Reson.*, 1978, **32**, 455.
132. H. J. Jakobsen, A. J. Zozulin, P. D. Ellis and J. D. Odom, *J. Magn. Reson.*, 1980, **38**, 219.
133. W. T. Raynes, *Mol. Phys.*, 1983, **49**, 443.
134. C. J. Jameson and H. J. Osten, *J. Chem. Phys.*, 1984, **81**, 4293.
135. C. J. Jameson and H. J. Osten, *J. Chem. Phys.*, 1984, **81**, 4300.
136. I. Paidarova, J. Komasa and J. Oddershede, *Mol. Phys.*, 1991, **72**, 559.
137. R. E. Wasylishen, J. O. Friedrich, S. Mooibroek and J. B. Macdonald, *J. Chem. Phys.*, 1985, **83**, 548.
138. H. P. A. Mercier, J. C. P. Saunders, G. J. Schrobilgen and S. S. Tsai, *Inorg. Chem.*, 1993, **32**, 386.
139. R. E. Wasylishen and N. Burford, *Can. J. Chem.*, 1987, **65**, 2707.
140. K. L. Leighton and R. E. Wasylishen, *Can. J. Chem.*, 1987, **65**, 1469.
141. H. J. Osten, C. J. Jameson and N. Craig, *J. Chem. Phys.*, 1985, **83**, 5434.
142. C. J. Jameson, D. Rehder and M. Hoch, *J. Am. Chem. Soc.*, 1987, **109**, 2589.
143. P. E. Hansen, *Ann. Rept NMR Spectrosc.*, 1983, **15**, 105.
144. Y. Nakashima, H. Kanada, M. Fukunaga, K. Suzuki and K. Takahashi, *Bull. Chem. Soc., Jpn*, 1992, **65**, 2894.
145. A. E. Aliev and K. D. M. Harris, *Magn. Reson. Chem.*, 1993, **31**, 54.

146. H. Kunzer, C. E. Cottrell and L. A. Paquette, *J. Am. Chem. Soc.*, 1986, **108**, 8089.
147. A. C. de Dios and C. J. Jameson, unpublished results.
148. T. G. Burlingame and W. H. Pirkle, *J. Am. Chem. Soc.*, 1966, **88**, 1837.
149. W. H. Pirkle, *J. Am. Chem. Soc.*, 1966, **88**, 1837.
150. R. Dyllick-Brenzinger and J. D. Roberts, *J. Am. Chem. Soc.*, 1980, **102**, 1166.
151. L. A. Silks, J. Peng, J. D. Odom and R. B. Dunlap, *J. Chem. Soc., Perkin Trans. 1*, 1991, 2495
152. A. D. Buckingham, T. Schaefer and W. G. Schneider, *J. Chem. Phys.*, 1960, **32**, 1227.
153. A. D. Buckingham and J. A. Pople, *Discuss. Faraday Soc.*, 1956, **22**, 17.
154. F. H. A. Rummens, in *NMR Basic Principles and Progress*, ed. P. Diehl, E. Fluck and R. Kosfeld, Springer-Verlag, Berlin, 1975, Vol. 10.
155. A. K. Jameson, C. J. Jameson and H. S. Gutowsky, *J. Chem. Phys.*, 1970, **53**, 2310.
156. C. J. Jameson, A. K. Jameson and S. M. Cohen, *J. Chem. Phys.*, 1975, **62**, 4224.
157. C. J. Jameson, A. K. Jameson and H. Parker, *J. Chem. Phys.*, 1978, **68**, 3943.
158. C. J. Jameson, A. K. Jameson and S. M. Cohen, *J. Chem. Phys.*, 1973, **59**, 4540.
159. C. J. Jameson, A. K. Jameson, D. Oppusunggu and S. Wille, *J. Chem. Phys.*, 1982, **76**, 152.
160. K. Jackowski, *Chem. Phys. Lett.*, 1992, **194**, 167.
161. C. J. Jameson, A. K. Jameson and D. Oppusunggu, *J. Chem. Phys.*, 1984, **81**, 2313.
162. C. J. Jameson, A. K. Jameson, S. M. Cohen, H. Parker, D. Oppusunggu, P. M. Burrell and S. Wille, *J. Chem. Phys.*, 1981, **74**, 1608.
163. J. C. Hindman, *J. Chem. Phys.*, 1966, **44**, 4582.
164. A. K. Jameson and C. J. Jameson, *Chem. Phys. Lett.*, 1987, **134**, 461.
165. M. Alei, A. E. Florin, W. M. Litchman and J. F. O'Brien, *J. Phys. Chem.*, 1971, **75**, 932.
166. C. J. Jameson and A. K. Jameson, *J. Chem. Phys.*, 1984, **81**, 1198.
167. C. J. Jameson, A. K. Jameson and D. Oppusunggu, *J. Chem. Phys.*, 1984, **87**, 85.
168. C. J. Jameson, A. K. Jameson and H. Parker, *J. Chem. Phys.*, 1979, **70**, 5916.
169. C. J. Jameson, A. K. Jameson and P. M. Burrell, *J. Chem. Phys.*, 1980, **73**, 6013.
170. G. Heckmann and E. Fluck, *Mol. Phys.*, 1972, **23**, 175.
171. D. Brinkman and H. Y. Carr, *Phys. Rev.*, 1966, **150**, 174.
172. W. W. Warren and R. E. Norberg, *Phys. Rev.*, 1966, **148**, 402.
173. R. K. Mazitov, K. M. Enikeev and A. V. Ilyasov, *Z. Phys. Chem.*, 1987, **155**, 55.
174. P. Diehl, O. Muenster and J. Jokisaari, *Chem. Phys. Lett.*, 1991, **178**, 147.
175. K. W. Miller, N. V. Reo, A. J. M. S. Uiterkamp, D. P. Stengle, T. R. Stengle and K. L. Williamson, *Proc. Natl Acad. Sci.* USA, 1981, **78**, 4946.
176. R. Seydoux, P. Diehl, R. K. Mazitov and J. Jokisaari, *J. Magn. Reson. A*, 1993, **101**, 78.
177. M. Haser, R. Ahlrichs, H. P. Baron, P. Weis and H. Horn, *Theo. Chim. Acta*, 1992, **83**, 455.
178. U. Meier, C. vanWüllen and M. Schindler, *J. Comput. Chem.*, 1992, **13**, 551.
179. P. Pulay, private communication.
180. D. B. Chesnut and K. D. Moore, *J. Comput. Chem.*, 1989, **10**, 648.
181. P. W. Fowler, P. Lazzeretti, M. Malagoli and R. Zanasi, *J. Phys. Chem.*, 1991, **95**, 6404.
182. D. B. Chesnut and C. G. Phung, *Chem. Phys. Lett.*, 1991, **183**, 505.
183. C. E. Dykstra and P. G. Jasien, *Chem. Phys. Lett.*, 1984, **109**, 388.
184. J. G. Pearson, E. Oldfield, F. S. Lee and A. Warshel, *J. Am. Chem. Soc.*, 1993, **115**, 6851.
185. A. D. McLean and G. S. Chandler, *J. Chem. Phys.*, 1980, **72**, 5639.
186. C. C. McDonald and W. D. Phillips, *J. Am. Chem. Soc.*, 1967, **89**, 6332.
187. A. Allerhand, R. F. Childers and E. Oldfield, *Biochemistry*, 1973, **12**, 1335.
188. J. D. Augspurger, C. E. Dykstra, E. Oldfield and J. G. Pearson, in *Nuclear Magnetic Shieldings and Molecular Structure*, ed. J. A. Tossell, NATO ASI Series C Vol. 386, Kluwer, Dordrecht, 1993, pp. 75–94.

189. F. S. Lee, Z. Chu and A. Warshel, *J. Comput. Chem.*, 1993, **14**, 161.
190. C. Lian, H. B. Le, B. Montez, J. Patterson, S. Harrell, D. Laws, I. Matsumura, J. Pearson and E. Oldfield, *Biochemistry*, 1994, **33**, 5238.
191. R. Chattopadhyaya, W. E. Meador, A. R. Means and F. A. Quiocho, *J. Mol. Biol.*, 1992, **228**, 1177.
192. P. J. Loll and E. E. Lattman, *Protein Struct. Funct. Genet.*, 1989, **5**, 183.
193. S. J. Weiner, P. A. Kollman, D. T. Nguyen and D. A. Case, *J. Comput. Chem.*, 1986, **7**, 230.